





## Complete and nondestructive distinguishment of many-body Rydberg entanglement via robust geometric quantum operations

F.-Q. Guo <sup>1</sup>, J.-L. Wu,<sup>2</sup> X.-Y. Zhu,<sup>1,3</sup> Z. Jin,<sup>4</sup> Y. Zeng <sup>5</sup>, S. Zhang,<sup>6</sup> L.-L. Yan,<sup>1,\*</sup> M. Feng <sup>1,7,8,†</sup> and S.-L. Su <sup>1,‡</sup>

<sup>1</sup>*School of Physics and Microelectronics, Key Laboratory of Materials Physics of Ministry of Education, Zhengzhou University, Zhengzhou 450052, China*

<sup>2</sup>*School of Physics, Harbin Institute of Technology, Harbin 150001, China*

<sup>3</sup>*College of Science, Henan University of Engineering, Zhengzhou, 451191, China*

<sup>4</sup>*School of Physics, Northeast University, Shenyang 110819, China*

<sup>5</sup>*School of Information Engineering, Zhengzhou University, Zhengzhou 450001, China*

<sup>6</sup>*Department of Physics, Yanbian University, Yanji 133002, China*

<sup>7</sup>*State Key Laboratory of Magnetic Resonance and Atomic and Molecular Physics, Wuhan Institute of Physics and Mathematics, Chinese Academy of Sciences, Wuhan 430071, China*

<sup>8</sup>*Department of Physics, Zhejiang Normal University, Jinhua 321004, China*



(Received 1 September 2020; accepted 9 November 2020; published 15 December 2020)

Practical application of quantum information requires distinguishing multipartite entanglement in a complete, nondestructive, and robust way. Here we explore the possibility to accomplish such a task using Rydberg atoms based on blockade effect and user-defined-passage-based geometric quantum logic gates. Our proposal focuses on distinguishing groups of many-body Greenberger-Horne-Zeilinger (GHZ) states and groups of cluster states, and for bipartite cases distinguishing Bell states, which are basic ingredients of quantum information processing. We validate our proposal by numerical results, showing complete and nondestructive accomplishment of distinguishing above multipartite entangled states and also robustness against decoherence. We exemplify two practical applications regarding quantum teleportation and quantum dense coding to demonstrate the value of our proposal. This idea is scalable and experimentally relevant and can be readily generalized to other quantum information candidates, such as superconducting circuits, NV centers, as well as trapped-ion systems with different-level structures.

DOI: [10.1103/PhysRevA.102.062410](https://doi.org/10.1103/PhysRevA.102.062410)

### I. INTRODUCTION

In view of the long coherence time of internal atomic states and strong Rydberg-Rydberg interaction (RRI), Rydberg atoms have become a particularly attractive platform for quantum computation [1]. One of the most fascinating phenomena caused by RRI is Rydberg blockade [1–9], which can suppress the excitation of other (ambient) Rydberg atoms when one atom is excited to the Rydberg state. Rydberg blockade, which has been observed experimentally [3,6], provides a way to implement fast quantum gates [1,7,10,11] and generate quantum entanglement [12]. The experimental progress [13–22] and very recent theoretical works [23–30] have demonstrated great potential applications of Rydberg atoms in quantum information processing. In addition, Rydberg atoms have many other dramatic effects, such as Rydberg antiblockade [31–38], and Rydberg dressing [39–41], which enrich the charm of Rydberg atoms as an excellent platform in quantum technology.

As one of the most famous entangled states, the Greenberger-Horne-Zeilinger (GHZ) state have exhibited

more profound nonlocality of quantum physics [42–44] than Bell state, applicable for quantum networks [45,46], quantum metrology [47], and measurement-based quantum computation [48–50]. Another vital entangled state is the cluster state [51], which is more stable than Bell and GHZ states and can be used in one-way quantum computation [52,53]. Hein *et al.* proved that the cluster states are resistant to decoherence [54]. Through some local operations, two- and three-qubit cluster states can be converted to Bell states and three-qubit GHZ states, respectively [51]; with more qubits involved, however, this state converting is not available by only local operations. Until now, various methods of preparing Bell states, GHZ states and cluster states have been developed [55–61], while the complete distinguishment of entangled states, an important operation for obtaining quantum state information, is still highly demanded [61–66]. In 1998, Pan and Zeilinger proposed the first practical GHZ-state analyzer with linear-optical elements, which can identify two of  $N$ -photon GHZ states [64]. On that basis, the entanglement distinguishment for photon systems [65,66] and superconducting systems [67] have also been studied. In Rydberg atom systems, however, distinguishing multipartite entangled states, such as GHZ states and cluster states, have not been studied yet.

On the other hand, geometric phases [68,69], which are insensitive to the evolution details but the whole process, are

\*llyan@zzu.edu.cn

†mangfeng@wipm.ac.cn

‡slsu@zzu.edu.cn

robust to local noises. Besides, to avoid decoherence caused by the interaction between the quantum system and environment, a series of quantum computation schemes based on Abelian or non-Abelian geometric phases [70–72] were proposed. However, the early geometric quantum computation was based on the geometric phase obtained by the adiabatic evolution [73–75], where the interaction between the system and the environment is of a long time, susceptible to decoherence and errors. Recently, schemes of nonadiabatic holonomic quantum computation (NHQC) [76–85] were proposed to avoid the long run-time requirement but share the robustness advantages of its adiabatic counterparts. Considering a quantum system with general time-dependent Hamiltonian  $\hat{H}(t)$  and assuming a time-dependent  $L$ -dimensional subspace  $\mathcal{S}(t)$  spanned by the orthonormal basis vectors  $\{|\phi_k(t)\rangle\}_{k=1}^L$  at each moment of time, where  $|\phi_k(t)\rangle$  satisfy the Schrödinger equation  $i\frac{d}{dt}|\phi_k(t)\rangle = \hat{H}(t)|\phi_k(t)\rangle$ , we have, for  $\{|\phi_k(t)\rangle\}$  at each instant  $t$ ,  $|\phi_k(t)\rangle = \hat{U}(t, 0)|\phi_k(0)\rangle$  with time evolution operator  $\hat{U}(t, 0) = \mathbf{T}e^{-i\int_0^t \hat{H}(t')dt'}$ ,  $\mathbf{T}$  being time ordering. If  $|\phi_k(t)\rangle$  satisfy (i)  $\sum_{k=1}^L |\phi_k(\tau)\rangle\langle\phi_k(\tau)| = \sum_{k=1}^L |\phi_k(0)\rangle\langle\phi_k(0)|$  and (ii)  $\langle\phi_k(t)|\hat{H}(t)|\phi_l(t)\rangle = 0$  ( $k, l = 1, \dots, L$ ), the unitary transformation  $\hat{U}(\tau, 0)$  is a holonomy matrix acting on  $L$ -dimensional subspace  $\mathcal{S}(0)$  spanned by  $\{|\phi_k(0)\rangle\}_{k=1}^L$  [76,77]. They are cyclic condition and parallel-transport condition of NHQC, respectively. Nevertheless, conventional NHQC gates need to meet strict conditions of achieving cyclic evolution [76,77], which reduces the robustness of the geometric quantum gates against control errors. To this end, Liu [86] *et al.* proposed alternate geometric gates named NHQC+, which only requires the accumulated dynamic phase being zero in the whole evolution process. This maintains the flexibility and error tolerance, but breaks the parallel-transport condition of the NHQC.

In this manuscript, based on geometric quantum operations, we propose schemes to completely distinguish entangled states in a nondestructive way. The nonadiabatic geometric gates on Rydberg atoms are constructed by NHQC+ [86] with the user-defined-passage-based pulse design [87]. Based on the constructed geometric quantum gates, we first construct parity discriminator and phase discriminators, and then realize distinguishment for Bell states,  $N$ -qubit GHZ states, as well as four- and five-qubit cluster states. Examples regarding quantum teleportation [88] and quantum dense coding [89] are given for practical application and significance of our entanglement discriminators.

The article is organized as follows. In Sec. II, robust Rydberg geometric quantum gates are introduced based on the user-defined passages. In Sec. III, we discuss the realization schemes of  $N$ -qubit Rydberg parity discriminator and entangled state phase discriminators, respectively. In Sec. IV, we construct nondestructive  $N$ -qubit entangled state discriminators by combining the presented parity discriminator and phase discriminators, then, Bell states,  $N$ -qubit GHZ states, four- and five-qubit cluster states will be distinguished completely. Besides, the discriminators can be employed in quantum teleportation and quantum dense coding as exemplified to simply demonstrate the practical applications. Sec. V is for discussion and conclusion.

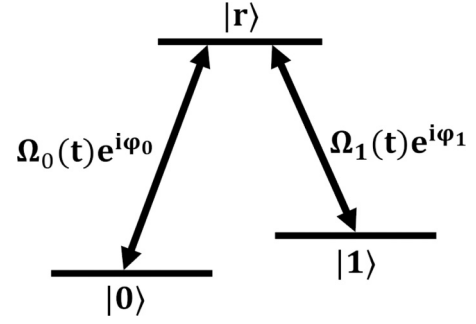


FIG. 1. Configuration diagram of Rydberg single-qubit gate.

## II. RYDBERG GEOMETRIC QUANTUM GATE

### A. Single-qubit gate

Now we show how to construct the single-qubit gate via NHQC+ dynamics. As sketched in Fig. 1, we consider a Rydberg atom with two stable ground states  $|0\rangle$ ,  $|1\rangle$  and a Rydberg state  $|r\rangle$ .  $|0\rangle$  and  $|1\rangle$  are coupled to  $|r\rangle$  with Rabi frequencies  $\Omega_0(t)e^{i\varphi_0}$  and  $\Omega_1(t)e^{i\varphi_1}$ , respectively, where  $\varphi_0$  and  $\varphi_1$  are time-independent phases. In the interaction picture, such a system in units of  $\hbar=1$  can be written as

$$\hat{H} = \frac{1}{2}[\Omega_0(t)|0\rangle\langle r|e^{i\varphi_0} + \Omega_1(t)|1\rangle\langle r|e^{i\varphi_1}] + \text{H.c.} \quad (1)$$

We choose two user-defined passages  $|\xi_0(t)\rangle$  and  $|\xi_1(t)\rangle$  and an orthogonal state  $|\xi_2(t)\rangle$  by defining some time-parameterized states (as input) for inversely engineering the driving Hamiltonian [87], as

$$\begin{aligned} |\xi_0(t)\rangle &= \cos\frac{\theta}{2}|0\rangle - \sin\frac{\theta}{2}e^{-i\varphi}|1\rangle, \\ |\xi_1(t)\rangle &= \left[ \cos\frac{\Theta}{2}e^{-i\alpha/2}\sin\frac{\theta}{2}e^{i\varphi}|0\rangle + \cos\frac{\Theta}{2}e^{-i\alpha/2}\cos\frac{\theta}{2}|1\rangle \right. \\ &\quad \left. + \sin\frac{\Theta}{2}e^{i\alpha/2}|r\rangle \right] e^{-i\gamma/2}, \\ |\xi_2(t)\rangle &= \left[ \sin\frac{\Theta}{2}e^{-i\alpha/2}\sin\frac{\theta}{2}e^{i\varphi}|0\rangle + \sin\frac{\Theta}{2}e^{-i\alpha/2}\cos\frac{\theta}{2}|1\rangle \right. \\ &\quad \left. - \cos\frac{\Theta}{2}e^{i\alpha/2}|r\rangle \right] e^{i\gamma/2}, \end{aligned} \quad (2)$$

where  $\Theta$ ,  $\alpha$ ,  $\theta$ ,  $\varphi$  are generally parameters to be determined below,  $\Omega = \sqrt{\Omega_0^2 + \Omega_1^2}$ ,  $\Omega_0/\Omega_1 = \tan(\theta/2)$ , and  $\varphi = \varphi_0 - \varphi_1$ . To achieve geometric gates in the computational subspace  $\{|0\rangle, |1\rangle\}$ , we impose the boundary condition  $\Theta(0) = \Theta(T) = 2n\pi$ ,  $n = 0, 1, 2, \dots$ . Therefore the time dependence of the control fields can be determined by the passages through solving the Schrödinger equation  $i\frac{d}{dt}|\psi(t)\rangle = H|\psi(t)\rangle$ ,

$$\begin{aligned} \Omega \cos \varphi_1 &= \cos \alpha \sin \Theta \dot{\gamma} - \sin \alpha \dot{\Theta}, \\ \Omega \sin \varphi_1 &= -\sin \alpha \sin \Theta \dot{\gamma} - \cos \alpha \dot{\Theta}, \\ \dot{\alpha} &= -\cos \Theta \dot{\gamma}. \end{aligned} \quad (3)$$

For  $\Theta(t)$  and  $\alpha(t)$ , a simple choice is to set  $\Theta = 2\pi\tau/t_f$ ,  $\gamma = 4\pi\tau/t_f$ ,  $\alpha = -2\sin\Theta$ , with  $\tau$  and  $t_f$  being the accumulated operation time and total operation time of this atom,

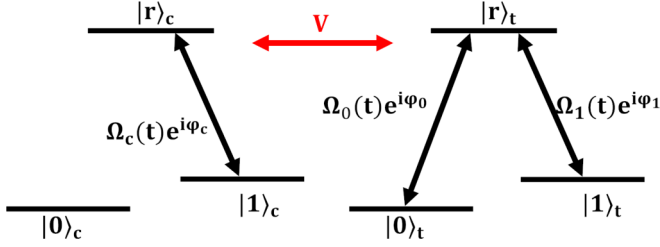


FIG. 2. Configurational diagram of Rydberg two-qubit CPG.

respectively.  $\theta$  and  $\varphi$  are set as time-independent parameters to be determined according to different geometric gates. Meanwhile, to get purely geometric phase under a cyclic evolution, we require the control pulses and user-defined passages satisfying the following condition,

$$\int_0^{t_f} \langle \xi_k(t) | \hat{H} | \xi_l(t) \rangle dt = 0, \quad k, l = 0, 1. \quad (4)$$

Next, we demonstrate how to build up geometric quantum gate. Let us start with the following set of basis states,  $\{|\xi_0\rangle, |\xi_1(0)\rangle\}$ . Note that these basis states can be spanned in the computational subspace  $\{|0\rangle, |1\rangle\}$  when  $\Theta = 0$ . Since  $\hat{H}|\xi_0\rangle = 0$  in the whole process, one can get  $\int_0^{t_f} \langle \xi_0(t) | \hat{H} | \xi_0(t) \rangle dt = \int_0^{t_f} \langle \xi_0(t) | \hat{H} | \xi_1(t) \rangle dt = 0$  easily. For  $\int_0^{t_f} \langle \xi_1(t) | \hat{H} | \xi_1(t) \rangle dt = 1/2 \int_0^{t_f} \Omega \sin \Theta (\cos \varphi_1 \cos \alpha - \sin \varphi_1 \sin \alpha) dt$ , we divide the process into two intervals. In the first interval ( $0 \leq t \leq t_f/2$ ), the corresponding evolution operator is  $\hat{U}_1(t_f/2, 0) = |\xi_0\rangle\langle \xi_0| + |\xi_1(t_f/2)\rangle\langle \xi_1(0)|$ ; In the second interval ( $t_f/2 \leq t \leq t_f$ ), the corresponding evolution operator is  $\hat{U}_2(t_f, t_f/2) = |\xi_0\rangle\langle \xi_0| + |\xi_1(t_f)\rangle\langle \xi_1(t_f/2)|$ , where a minus sign is suddenly applied to  $\Omega$  and  $\varphi_1$  at the beginning of the second interval to eliminate the dynamical accumulation of the phase. Thus the final evolution operator is  $\hat{U}(t_f, 0) \equiv \hat{U}_0 = |\xi_0\rangle\langle \xi_0| - |\xi_1(0)\rangle\langle \xi_1(0)|$ , leading to a geometric single-qubit gate in the computational subspace  $\{|0\rangle, |1\rangle\}$  as

$$\hat{U}_0 = \begin{pmatrix} \cos \theta & -\sin \theta e^{i\varphi} \\ -\sin \theta e^{-i\varphi} & -\cos \theta \end{pmatrix}. \quad (5)$$

General single-qubit logical operations can be achieved, based on Eq. (5), by setting different values of  $\theta$  and  $\varphi$ .

### B. Two-qubit gate

Figure 2 sketches two identical Rydberg atoms under the vdW interaction Hamiltonian  $H_r = V|rr\rangle\langle rr|$ , where each atom consists of two stable ground states  $|0\rangle, |1\rangle$  and a Rydberg state  $|r\rangle$ , and the subscript “c” (“t”) denotes the control (target) atom.  $|1\rangle_c$  and  $|0\rangle_t$  ( $|1\rangle_t$ ) are coupled to  $|r\rangle_c$  and  $|r\rangle_t$  by Rabi frequencies  $\Omega_c(t)e^{i\varphi_c}$  and  $\Omega_0(t)e^{i\varphi_0}$  [ $\Omega_1(t)e^{i\varphi_1}$ ], respectively, where  $\varphi_c, \varphi_0$ , and  $\varphi_1$  are time-independent laser phases. The target atom can be described by Eq. (1), while the control atom is governed by

$$\hat{H}_c = \frac{1}{2}\Omega_c(t)|1\rangle_c\langle r|e^{i\varphi_c} + \text{H.c.} \quad (6)$$

Equation (6) would have the similar form to Eq. (1) if  $\Omega_0 = 0$  is satisfied in Eq. (1). Thus one can use the similar user-defined passage to design the NHQC+ dynamics based on

Eq. (6). On that basis, the two-qubit gate can be constructed by three steps as follows, and the NHQC+ conditions are satisfied after accomplishing all the steps.

Step (i). In the time interval  $[0, t_f/2]$ , excite the control atom to  $|r\rangle_c$  if its state is  $|1\rangle_c$  initially and the condition  $\int \Omega_c d\tau = \pi$  is satisfied.

Step (ii). Perform the single-qubit geometric operations on the target atom in the time interval  $[t_f/2, 3t_f/2]$ , as shown in Sec. II A. The process could be classified as two types [90]. Type I. When control atom is initially in state  $|0\rangle_c$ , it is not excited after step (i), so the operations on the target atom will work validly in step (ii) similar to the process in Sec. II A. Type II. When the control atom is initially in state  $|1\rangle_c$ , it is excited to Rydberg state  $|r\rangle_c$  after Step (i), the operations on the target atom would not work due to Rydberg blockade [2,90] with condition  $V \gg \Omega$ .

Step (iii) In the time interval  $[3t_f/2, 2t_f]$ , perform an operation similar to Step (i) to de-excite the control atom from  $|r\rangle_c$  to  $|1\rangle_c$  under the condition  $\int \Omega_c d\tau = \pi$ .

The operation  $\hat{U} = |0\rangle_c\langle 0| \otimes \hat{U}_0 + |1\rangle_c\langle 1| \otimes \hat{I}$  will be achieved after finishing all the three steps with total time  $2t_f$ . It should be noted that the cyclic condition of NHQC+ is not satisfied for the evolution process of step (i) or step (iii) on the control atom. Nevertheless, for the whole process consisting of steps (i)–(iii), the conditions of NHQC+ are well satisfied. Firstly, the state evolution of the target atom in step (ii) can be proved to satisfy the NHQC+ conditions based on Sec. II A. Secondly, the whole evolution process of the control atom in steps (i) and (iii) satisfies the cyclic condition as well as the accumulated dynamic phase being zero, like the process in Sec. II A. It should be noted that we need to add a minus sign suddenly on  $\varphi_c$  at  $3t_f/2$  to ensure that the dynamic phase can be eliminated and the evolution process  $|1\rangle_c \rightarrow |1\rangle_c$  can be completed.

Similarly, if Hamiltonian of the control atom is redesigned as  $\hat{H}_c = \frac{1}{2}\Omega_c(t)|0\rangle_c\langle r|e^{i\varphi_c} + \text{H.c.}$ , the operation  $\hat{U} = |0\rangle_c\langle 0| \otimes \hat{I} + |1\rangle_c\langle 1| \otimes \hat{U}_0$  will be achieved.

## III. MULTIQUBIT PARITY DISCRIMINATOR AND PHASE DISCRIMINATORS

Here we illustrate how to realize  $N$ -qubit parity discriminator and phase discriminators.

### A. Multiqubit Rydberg parity discriminator

Firstly, we define the parity to distinguish whether our state is of odd or even parity. If a state of  $N$  qubits can be expressed as  $|\zeta_1\zeta_2\cdots\zeta_N\rangle$  with  $\zeta \in \{0, 1\}$ , we can set  $S = \sum_{i=1}^N \zeta_i \oplus$ , where  $\oplus$  denotes the summing modulo 2 of all the single states. The  $N$ -qubit state is of even parity when the result of  $S$  is 0 while odd parity when the result of  $S$  is 1. For instance, for the two-qubit state  $|11\rangle$ , the result is  $S = 0$ , so  $|11\rangle$  is of even parity. But for the three-qubit state,  $|111\rangle$  is of odd parity due to  $S = 1$ . Secondly, we need a two-qubit gate with  $\theta = 0, \varphi = 0$ , i.e., a controlled-Z gate/ $\pi$  controlled-phase gate (CPG):  $\hat{U}_{\text{CPG}} = |0\rangle_c\langle 0| \otimes \hat{U}_z + |1\rangle_c\langle 1| \otimes \hat{I}$ , where the operator  $\hat{U}_z = \begin{pmatrix} 1 & 0 \\ 0 & -1 \end{pmatrix}$  is for a Pauli Z gate. We now show the way to realize a multi-qubit parity discriminator with the

operation  $\hat{U}_{\text{CPG}}$ . An  $N$ -qubit initial state can be written as

$$|\Psi\rangle = \sum_{i=1}^{2^{N-1}} (\alpha_i |O\rangle_i + \beta_i |E\rangle_i), \quad (7)$$

where  $|O\rangle_i$  denotes an odd-parity state,  $|E\rangle_i$  an even-parity state, and  $\sum_{i=1}^{2^{N-1}} (|\alpha_i|^2 + |\beta_i|^2) = 1$ .

Next, we utilize an auxiliary Rydberg atom A with the initial state  $\frac{1}{\sqrt{2}}(|0\rangle_a + |1\rangle_a)$  to control the change of systematic atoms sequentially. The operational process is given by

$$\begin{aligned} & |\Psi\rangle \otimes \frac{1}{\sqrt{2}}(|0\rangle_a + |1\rangle_a) \\ & \xrightarrow{\hat{U}_{\text{CPG}}^N, \dots, \hat{U}_{\text{CPG}}^1} \sum_{i=1}^{2^{N-1}} \alpha_i |O\rangle_i \otimes \frac{1}{\sqrt{2}}(|1\rangle_a - |0\rangle_a) \\ & + \sum_{i=1}^{2^{N-1}} \beta_i |E\rangle_i \otimes \frac{1}{\sqrt{2}}(|0\rangle_a + |1\rangle_a), \end{aligned} \quad (8)$$

where  $\hat{U}_{\text{CPG}}^i$  ( $i = 1, 2, \dots, N$ ) is the operation on atom  $i$  and the auxiliary atom. Then the auxiliary atom A can be detected after performing a Hadamard operation  $(|1\rangle_a + |0\rangle_a)/\sqrt{2} \rightarrow |0\rangle_a$  and  $(|0\rangle_a - |1\rangle_a)/\sqrt{2} \rightarrow |1\rangle_a$ . If the auxiliary atom A is detected in  $|1\rangle_a$ , the systematic state projected on a multi-atom state is of odd parity. If the atom A is in  $|0\rangle_a$ , the systematic state is of even parity. For clarity, we take a two-qubit parity discriminator as an example. The two-qubit systematic initial state can be written as [62,91]

$$|\Psi\rangle_{12} = \alpha|00\rangle_{12} + \beta|01\rangle_{12} + \gamma|10\rangle_{12} + \delta|11\rangle_{12}, \quad (9)$$

with  $|\alpha|^2 + |\beta|^2 + |\gamma|^2 + |\delta|^2 = 1$ . Regarding the auxiliary atom as a control atom and the two systematic atoms as the target atoms to perform  $\hat{U}_{\text{CPG}}$  operations. The result is given by

$$\begin{aligned} & |\Psi\rangle_{12} \otimes \frac{1}{\sqrt{2}}(|0\rangle_a + |1\rangle_a) \\ & \xrightarrow{\hat{U}_{\text{CPG}}^2, \hat{U}_{\text{CPG}}^1} (\alpha|00\rangle_{12} + \delta|11\rangle_{12}) \otimes \frac{1}{\sqrt{2}}(|0\rangle_a + |1\rangle_a) \\ & + (\beta|01\rangle_{12} + \gamma|10\rangle_{12}) \otimes \frac{1}{\sqrt{2}}(|1\rangle_a - |0\rangle_a). \end{aligned} \quad (10)$$

If the measurement result of the auxiliary atom is in state  $\frac{1}{\sqrt{2}}(|0\rangle_a + |1\rangle_a)$ , the systematic state is of even parity with  $\alpha|00\rangle_{12} + \delta|11\rangle_{12}$ . If the measurement result is in state  $\frac{1}{\sqrt{2}}(|1\rangle_a - |0\rangle_a)$ , the systematic state is of odd parity with  $\beta|01\rangle_{12} + \gamma|10\rangle_{12}$ . For a  $N$ -qubit state, we implement the operation  $\hat{U}_{\text{CPG}}$  to each atom.

### B. GHZ-state Rydberg phase discriminator

For the GHZ-state phase discriminator of Rydberg atoms, a two-qubit controlled-NOT (CNOT) gate is needed, which is constructed by setting  $\theta = \pi/2$  and  $\varphi = \pi$ :  $\hat{U}_{\text{CNOT}} = |0\rangle_c\langle 0| \otimes \hat{U}_x + |1\rangle_c\langle 1| \otimes \hat{I}$ , where the operator  $\hat{U}_x = \begin{pmatrix} 0 & 1 \\ 1 & 0 \end{pmatrix}$  is for a Pauli X gate. Beyond that, before discussing the construction of the GHZ-state Rydberg phase discriminator,

we show a Rydberg discriminator with special ability to distinguish  $|\Psi^\pm\rangle$ , which is given by

$$\begin{aligned} |\Psi^+\rangle &= \alpha(|\mu_1 \cdots \mu_N\rangle + |\bar{\mu}_1 \cdots \bar{\mu}_N\rangle) \\ &\quad \pm \beta(|\nu_1 \cdots \nu_N\rangle + |\bar{\nu}_1 \cdots \bar{\nu}_N\rangle), \\ |\Psi^-\rangle &= \alpha(|\mu_1 \cdots \mu_N\rangle - |\bar{\mu}_1 \cdots \bar{\mu}_N\rangle) \\ &\quad \pm \beta(|\nu_1 \cdots \nu_N\rangle - |\bar{\nu}_1 \cdots \bar{\nu}_N\rangle), \end{aligned}$$

where  $\mu, \nu \in \{0, 1\}$ ,  $\bar{\mu}_i = 1 - \mu_i$ ,  $\bar{\nu}_i = 1 - \nu_i$  ( $i = 1, 2, \dots, N$ ). If we carry out these operations  $\hat{U}_{\text{CNOT}}^1, \dots, \hat{U}_{\text{CNOT}}^N$  with an auxiliary atom prepared initially in  $\frac{1}{\sqrt{2}}(|0\rangle_a + |1\rangle_a)$ , we can get

$$\begin{aligned} & |\Psi^+\rangle \otimes \frac{1}{\sqrt{2}}(|0\rangle_a + |1\rangle_a) \\ & \xrightarrow{\hat{U}_{\text{CNOT}}^N, \dots, \hat{U}_{\text{CNOT}}^1} |\Psi^+\rangle \otimes \frac{1}{\sqrt{2}}(|0\rangle_a + |1\rangle_a), \\ & |\Psi^-\rangle \otimes \frac{1}{\sqrt{2}}(|0\rangle_a + |1\rangle_a) \\ & \xrightarrow{\hat{U}_{\text{CNOT}}^N, \dots, \hat{U}_{\text{CNOT}}^1} |\Psi^-\rangle \otimes \frac{1}{\sqrt{2}}(|1\rangle_a - |0\rangle_a). \end{aligned} \quad (11)$$

The detailed calculation can be found in Appendix A.

The GHZ-state phase discriminator can be regarded as a special case of Eq. (11). For clarity and to show GHZ-state Rydberg phase discriminator, we take eight three-qubit GHZ states as an example, which read

$$\begin{aligned} |\Psi_0^\pm\rangle_{123} &= \frac{1}{\sqrt{2}}(|000\rangle \pm |111\rangle), \\ |\Psi_1^\pm\rangle_{123} &= \frac{1}{\sqrt{2}}(|100\rangle \pm |011\rangle), \\ |\Psi_2^\pm\rangle_{123} &= \frac{1}{\sqrt{2}}(|010\rangle \pm |101\rangle), \\ |\Psi_3^\pm\rangle_{123} &= \frac{1}{\sqrt{2}}(|001\rangle \pm |110\rangle). \end{aligned} \quad (12)$$

We can express them in another way as  $|\Psi_i^\pm\rangle_{123} = \frac{1}{\sqrt{2}}(|\mu\nu\chi\rangle \pm |\bar{\mu}\bar{\nu}\bar{\chi}\rangle)$ , where  $\mu, \nu, \chi \in \{0, 1\}$ ,  $\bar{\mu} = 1 - \mu$ ,  $\bar{\nu} = 1 - \nu$ ,  $\bar{\chi} = 1 - \chi$ , and assume that the auxiliary atomic state is initially in  $\frac{1}{\sqrt{2}}(|0\rangle_a + |1\rangle_a)$ . The process of the scheme is

$$\begin{aligned} & |\Psi_i^+\rangle_{123} \otimes \frac{1}{\sqrt{2}}(|0\rangle_a + |1\rangle_a) \\ & \xrightarrow{\hat{U}_{\text{CNOT}}^3, \hat{U}_{\text{CNOT}}^2, \hat{U}_{\text{CNOT}}^1} |\Psi_i^+\rangle_{123} \otimes \frac{1}{\sqrt{2}}(|0\rangle_a + |1\rangle_a), \quad (13) \\ & |\Psi_i^-\rangle_{123} \otimes \frac{1}{\sqrt{2}}(|0\rangle_a + |1\rangle_a) \\ & \xrightarrow{\hat{U}_{\text{CNOT}}^3, \hat{U}_{\text{CNOT}}^2, \hat{U}_{\text{CNOT}}^1} |\Psi_i^-\rangle_{123} \otimes \frac{1}{\sqrt{2}}(|1\rangle_a - |0\rangle_a). \quad (14) \end{aligned}$$

Finally, we detect the state of the auxiliary atom. If the measurement result is  $\frac{1}{\sqrt{2}}(|0\rangle_a + |1\rangle_a)$ , the systematic state is  $|\Psi_i^+\rangle_{123}$ . Otherwise, if the result is  $\frac{1}{\sqrt{2}}(|1\rangle_a - |0\rangle_a)$ ,

the systematic state is  $|\Psi_i^-\rangle_{123}$ . Similarly, the four Bell states  $|\Psi_0^\pm\rangle_{12} = \frac{1}{\sqrt{2}}(|00\rangle \pm |11\rangle)$  and  $|\Psi_1^\pm\rangle_{12} = \frac{1}{\sqrt{2}}(|01\rangle \pm |10\rangle)$  can also be distinguished by this method.

### C. Four- and five-qubit cluster-state Rydberg phase discriminators

The term ‘‘cluster state’’ is first proposed by Briegel and Raussendorf [51], and the one-dimensional standard form reads

$$|\Psi\rangle_N = \frac{1}{\sqrt{2^N}} \bigotimes_{i=1}^N (|0\rangle_i + |1\rangle_i \hat{\sigma}_z^{i+1}),$$

where  $\hat{\sigma}_z$  (or  $\hat{U}_z$ ) denotes the Pauli Z operator and  $\hat{\sigma}_z^{N+1} \equiv \hat{I}$ . For  $N = 4$ , the general form of four-qubit cluster state is

$$|\Psi\rangle_4 = \frac{1}{2}(|0000\rangle + |0011\rangle + |1100\rangle - |1111\rangle). \quad (15)$$

Based on Eq. (15), a set of orthogonal basis can be constructed by corresponding local unitary operations:

$$\begin{aligned} |\Psi_1^{\mu\nu}\rangle &= \frac{1}{2}(|0\mu 0\nu\rangle + |0\mu 1\bar{\nu}\rangle + |1\bar{\mu} 0\nu\rangle - |1\bar{\mu} 1\bar{\nu}\rangle), \\ |\Psi_2^{\mu\nu}\rangle &= \frac{1}{2}(|0\mu 0\nu\rangle + |0\mu 1\bar{\nu}\rangle - |1\bar{\mu} 0\nu\rangle + |1\bar{\mu} 1\bar{\nu}\rangle), \\ |\Psi_3^{\mu\nu}\rangle &= \frac{1}{2}(|0\mu 0\nu\rangle - |0\mu 1\bar{\nu}\rangle + |1\bar{\mu} 0\nu\rangle + |1\bar{\mu} 1\bar{\nu}\rangle), \\ |\Psi_4^{\mu\nu}\rangle &= \frac{1}{2}(|0\mu 0\nu\rangle - |0\mu 1\bar{\nu}\rangle - |1\bar{\mu} 0\nu\rangle - |1\bar{\mu} 1\bar{\nu}\rangle), \end{aligned}$$

where  $\mu, \nu \in \{0, 1\}$ ,  $\bar{\mu} = 1 - \mu$ ,  $\bar{\nu} = 1 - \nu$ . For distinguishment of four-qubit cluster-state phase, two similar discriminators will be constructed. For the first four-qubit cluster-state phase discriminator, we carry out  $\hat{U}_{CNOT}^1$  and  $\hat{U}_{CNOT}^2$  and  $\hat{U}_{CPG}^3$ , where  $\hat{U}_{CPG} = |0\rangle_c\langle 0| \otimes \hat{I} + |1\rangle_c\langle 1| \otimes \hat{U}_z$ . This distinguishment process (see Appendix B) can be shown as

$$\begin{aligned} &|\Psi_1^{\mu\nu}\rangle \otimes \frac{1}{\sqrt{2}}(|0\rangle_a + |1\rangle_a) \\ &\xrightarrow{\hat{U}_{CPG}^3 \hat{U}_{CNOT}^2 \hat{U}_{CNOT}^1} |\Psi_3^{\mu\nu}\rangle \otimes \frac{1}{\sqrt{2}}(|0\rangle_a + |1\rangle_a), \end{aligned}$$

$$\begin{aligned} &|\Psi_2^{\mu\nu}\rangle \otimes \frac{1}{\sqrt{2}}(|0\rangle_a + |1\rangle_a) \\ &\xrightarrow{\hat{U}_{CPG}^3 \hat{U}_{CNOT}^2 \hat{U}_{CNOT}^1} |\Psi_4^{\mu\nu}\rangle \otimes \frac{1}{\sqrt{2}}(|1\rangle_a - |0\rangle_a). \end{aligned}$$

When we distinguish the states  $|\Psi_3^{\mu\nu}\rangle$  and  $|\Psi_4^{\mu\nu}\rangle$  with the auxiliary initial state  $\frac{1}{\sqrt{2}}(|0\rangle_a + |1\rangle_a)$ , we acquire the results  $|\Psi_1^{\mu\nu}\rangle$  with  $\frac{1}{\sqrt{2}}(|0\rangle_a + |1\rangle_a)$  and  $|\Psi_2^{\mu\nu}\rangle$  with  $\frac{1}{\sqrt{2}}(|1\rangle_a - |0\rangle_a)$ .

For the second phase discriminator, we carry out  $\hat{U}_{CNOT}^3$ ,  $\hat{U}_{CNOT}^4$ , and  $\hat{U}_{CPG}^1$  in sequence, where  $\hat{U}_{CPG} = |0\rangle_c\langle 0| \otimes \hat{I} + |1\rangle_c\langle 1| \otimes \hat{U}_z$ . The distinguishment process is given by

$$\begin{aligned} &|\Psi_1^{\mu\nu}\rangle \otimes \frac{1}{\sqrt{2}}(|0\rangle_a + |1\rangle_a) \\ &\xrightarrow{\hat{U}_{CPG}^1 \hat{U}_{CNOT}^4 \hat{U}_{CNOT}^3} |\Psi_2^{\mu\nu}\rangle \otimes \frac{1}{\sqrt{2}}(|0\rangle_a + |1\rangle_a), \end{aligned}$$

$$\begin{aligned} &|\Psi_3^{\mu\nu}\rangle \otimes \frac{1}{\sqrt{2}}(|0\rangle_a + |1\rangle_a) \\ &\xrightarrow{\hat{U}_{CPG}^1 \hat{U}_{CNOT}^4 \hat{U}_{CNOT}^3} |\Psi_4^{\mu\nu}\rangle \otimes \frac{1}{\sqrt{2}}(|1\rangle_a - |0\rangle_a). \end{aligned}$$

When we distinguish the states  $|\Psi_2^{\mu\nu}\rangle$  and  $|\Psi_4^{\mu\nu}\rangle$  with the auxiliary state  $\frac{1}{\sqrt{2}}(|0\rangle_a + |1\rangle_a)$ , we can also acquire the results  $|\Psi_1^{\mu\nu}\rangle$  with  $\frac{1}{\sqrt{2}}(|0\rangle_a + |1\rangle_a)$  and  $|\Psi_3^{\mu\nu}\rangle$  with  $\frac{1}{\sqrt{2}}(|1\rangle_a - |0\rangle_a)$ .

For  $N = 5$ , the general form of five-qubit cluster state is

$$|\Psi\rangle_5 = \frac{1}{2}(|00000\rangle + |00111\rangle + |11101\rangle + |11010\rangle).$$

We can also construct orthogonal basis by corresponding local unitary operations:

$$\begin{aligned} |\Psi_1^{\mu\nu\lambda}\rangle &= \frac{1}{2}(|0\mu 0\nu\lambda\rangle + |0\mu 1\bar{\nu}\bar{\lambda}\rangle + |1\bar{\mu} 1\nu\bar{\lambda}\rangle + |1\bar{\mu} 0\bar{\nu}\lambda\rangle), \\ |\Psi_2^{\mu\nu\lambda}\rangle &= \frac{1}{2}(|0\mu 0\nu\lambda\rangle - |0\mu 1\bar{\nu}\bar{\lambda}\rangle + |1\bar{\mu} 1\nu\bar{\lambda}\rangle - |1\bar{\mu} 0\bar{\nu}\lambda\rangle), \\ |\Psi_3^{\mu\nu\lambda}\rangle &= \frac{1}{2}(|0\mu 0\nu\lambda\rangle + |0\mu 1\bar{\nu}\bar{\lambda}\rangle - |1\bar{\mu} 1\nu\bar{\lambda}\rangle - |1\bar{\mu} 0\bar{\nu}\lambda\rangle), \\ |\Psi_4^{\mu\nu\lambda}\rangle &= \frac{1}{2}(|0\mu 0\nu\lambda\rangle - |0\mu 1\bar{\nu}\bar{\lambda}\rangle - |1\bar{\mu} 1\nu\bar{\lambda}\rangle + |1\bar{\mu} 0\bar{\nu}\lambda\rangle), \end{aligned}$$

where  $\mu, \nu, \lambda \in \{0, 1\}$ ,  $\bar{\mu} = 1 - \mu$ ,  $\bar{\nu} = 1 - \nu$ ,  $\bar{\lambda} = 1 - \lambda$ . For distinguishing five-qubit cluster-state phase, we obtain two discriminators by specifically distinguishing three-qubit states, which can be regarded as another special case of Eq. (11). Let's take  $|\Psi_3^{\mu\nu\lambda}\rangle$  as an example, which can be rewritten in two ways as

$$\begin{aligned} |\Psi_3^{\mu\nu\lambda}\rangle &= |0\mu\rangle_{12}(|0\nu\lambda\rangle + |1\bar{\nu}\bar{\lambda}\rangle)_{345} - |1\bar{\mu}\rangle_{12}(|1\nu\bar{\lambda}\rangle \\ &\quad + |0\bar{\nu}\lambda\rangle)_{345}, \\ &= |0\lambda\rangle_{35}(|0\mu\nu\rangle - |1\bar{\mu}\bar{\nu}\rangle)_{124} + |1\bar{\lambda}\rangle_{35}(|0\mu\bar{\nu}\rangle \\ &\quad - |1\bar{\mu}\nu\rangle)_{124}. \end{aligned}$$

When the initial state of the auxiliary atom is still  $\frac{1}{\sqrt{2}}(|0\rangle_a + |1\rangle_a)$ , if we carry out  $\hat{U}_{CNOT}^3$ ,  $\hat{U}_{CNOT}^4$  and  $\hat{U}_{CNOT}^5$ , we may detect the auxiliary atom to be in  $\frac{1}{\sqrt{2}}(|0\rangle_a + |1\rangle_a)$ . In another case, if we carry out  $\hat{U}_{CNOT}^1$ ,  $\hat{U}_{CNOT}^2$ , and  $\hat{U}_{CNOT}^4$ , we find the auxiliary atom is in  $\frac{1}{\sqrt{2}}(|1\rangle_a - |0\rangle_a)$ .

## IV. NONDESTRUCTIVE $N$ -QUBIT ENTANGLEMENT DISCRIMINATORS

Here we construct nondestructive  $N$ -Rydberg-atom entangled-state discriminators by combining the above parity discriminator and phase discriminators.

### A. GHZ-State and Bell-state Rydberg discriminators

We first show how to construct nondestructive  $N$ -qubit GHZ-state discriminator. As shown in Fig. 3(a), we can distinguish GHZ states by the two steps as below. Step (i), the phase information can be detected by GHZ-state phase discriminator. Step (ii), the parity information can be detected by GHZ-state parity discriminators, in which each parity discriminator check the parity information of two adjacent atoms. Both parity and phase information can be reflected by the measurement results of the auxiliary atom, and then the GHZ states can be distinguished completely without entanglement collapse. Take the distinguishment of eight GHZ states in

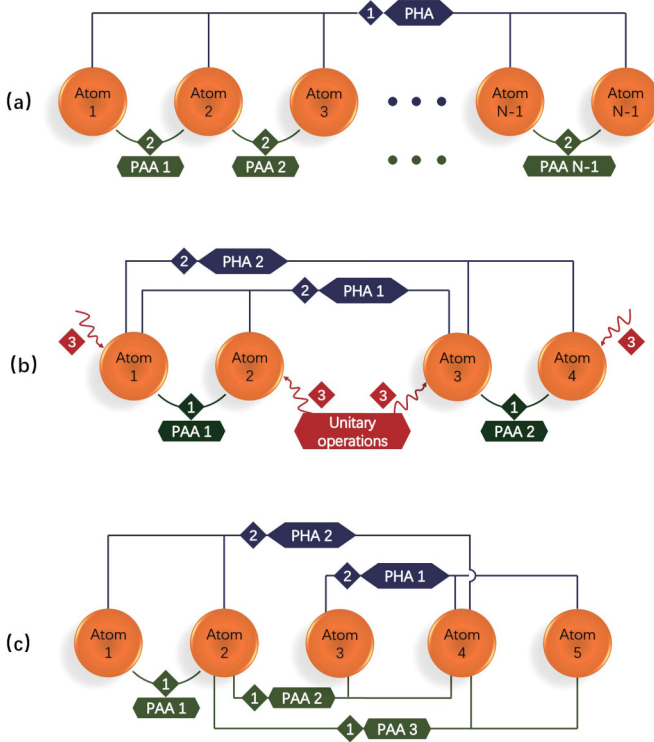


FIG. 3. Schematic diagrams of (a)  $N$ -qubit GHZ-state discriminator, (b) four-qubit cluster-state discriminator, (c) five-qubit cluster-state discriminator, where PAD denotes different parity discriminators and PHD denotes different phase discriminators for different tasks, for example, GHZ-state phase discriminator in (a). The numbers in the diamond represent the operation steps of the discriminator.

Eq. (12) as an example. With the phase information obtained, we divide the  $|\Psi_i^\pm\rangle_{123}$  into  $|\Psi_i^+\rangle_{123}$  and  $|\Psi_i^-\rangle_{123}$  after step (i). Applying the parity discriminators on atoms 1 and 2 as well as atoms 2 and 3 in step (ii), we further divide  $|\Psi_i^+\rangle_{123}$  into  $|\Psi_0^+\rangle_{123}$ ,  $|\Psi_1^+\rangle_{123}$ ,  $|\Psi_2^+\rangle_{123}$  and  $|\Psi_3^+\rangle_{123}$ , as well as  $|\Psi_i^-\rangle_{123}$  into  $|\Psi_0^-\rangle_{123}$ ,  $|\Psi_1^-\rangle_{123}$ ,  $|\Psi_2^-\rangle_{123}$  and  $|\Psi_3^-\rangle_{123}$ , completely distinguishing these eight GHZ states. The relationships between the measurement results of the auxiliary atom and the information of phase and parity can be obtained from Eqs. (13) and (10). We list the distinguishment results of the three-qubit GHZ states in Table I, in which  $|+\rangle_a \equiv \frac{1}{\sqrt{2}}(|0\rangle_a + |1\rangle_a)$  and  $|-\rangle_a \equiv \frac{1}{\sqrt{2}}(|1\rangle_a - |0\rangle_a)$ .

Similarly, the parity and phase information of four Bell states  $|\Psi_i^\pm\rangle_{12}$ , where  $i \in \{0, 1\}$ , can also be completely distinguished in these steps, and the results are shown in Table II.

## B. Four- and five-qubit cluster-state Rydberg discriminators

Here we present the distinguishment process of four-qubit cluster state, as shown in Fig. 3(b). Step(i), the parity discriminator on atoms 1 and 2 (PAD1) and parity discriminator on atoms 3 and 4 (PAD2) can detect each four-qubit cluster-state parity information. After PAD1, we divide the state  $|\Psi_i^{\mu\nu}\rangle$  into  $|\Psi_i^{0\nu}\rangle$  and  $|\Psi_i^{1\nu}\rangle$ , where  $i \in \{1, 2, 3, 4\}$ . After PAD2, we further divide  $|\Psi_i^{0\nu}\rangle$  into  $|\Psi_i^{00}\rangle$  and  $|\Psi_i^{01}\rangle$  as well as  $|\Psi_i^{1\nu}\rangle$  into  $|\Psi_i^{10}\rangle$  and  $|\Psi_i^{11}\rangle$ . Step(ii), after our cluster-state phase

TABLE I. The corresponding relationship between different initial GHZ states and the measurement results of the auxiliary atom, in which  $|+\rangle_a \equiv \frac{1}{\sqrt{2}}(|0\rangle_a + |1\rangle_a)$  and  $|-\rangle_a \equiv \frac{1}{\sqrt{2}}(|1\rangle_a - |0\rangle_a)$ .

Initial GHZ state	Measurement result		
	PHD	PAD1	PAD2
$ \Psi_0^+\rangle_{123} = \frac{1}{\sqrt{2}}( 000\rangle +  111\rangle)$	$ +\rangle_a$	$ +\rangle_a$	$ +\rangle_a$
$ \Psi_0^-\rangle_{123} = \frac{1}{\sqrt{2}}( 000\rangle -  111\rangle)$	$ -\rangle_a$	$ +\rangle_a$	$ +\rangle_a$
$ \Psi_1^+\rangle_{123} = \frac{1}{\sqrt{2}}( 100\rangle +  011\rangle)$	$ +\rangle_a$	$ -\rangle_a$	$ +\rangle_a$
$ \Psi_1^-\rangle_{123} = \frac{1}{\sqrt{2}}( 100\rangle -  011\rangle)$	$ -\rangle_a$	$ -\rangle_a$	$ +\rangle_a$
$ \Psi_2^+\rangle_{123} = \frac{1}{\sqrt{2}}( 010\rangle +  101\rangle)$	$ +\rangle_a$	$ -\rangle_a$	$ -\rangle_a$
$ \Psi_2^-\rangle_{123} = \frac{1}{\sqrt{2}}( 010\rangle -  101\rangle)$	$ -\rangle_a$	$ -\rangle_a$	$ -\rangle_a$
$ \Psi_3^+\rangle_{123} = \frac{1}{\sqrt{2}}( 001\rangle +  110\rangle)$	$ +\rangle_a$	$ +\rangle_a$	$ -\rangle_a$
$ \Psi_3^-\rangle_{123} = \frac{1}{\sqrt{2}}( 001\rangle -  110\rangle)$	$ -\rangle_a$	$ +\rangle_a$	$ -\rangle_a$

discriminator on atoms 1, 2, and 3 (PHD1) and cluster-state phase discriminator on atoms 3, 4, and 1 (PHD2), the phase information of cluster states can be determined, for example, after PHD1 and PHD2,  $|\Psi_i^{00}\rangle$  will be divided into  $|\Psi_1^{00}\rangle$ ,  $|\Psi_2^{00}\rangle$ ,  $|\Psi_3^{00}\rangle$ , and  $|\Psi_4^{00}\rangle$ , which can be determined by observing the two times measurement results of the auxiliary atom in Sec. III C. Distinguishing other twelve four-qubit cluster states is similar to this process. Generally, the cluster-state parity discriminators determine states with superscript  $\mu$  and  $\nu$ , the phase discriminators determine states with subscript  $i$ . Combining the cluster-state discriminators for parity and phase, all four-qubit cluster states can be completely distinguished. Step (iii), different from distinguishment of GHZ and Bell state, the initial state changes after completing the distinguishment of four-qubit cluster state. So we need further unitary operation to restore each initial state. For example,  $|\Psi_2^{00}\rangle$  will become  $|\Psi_4^{00}\rangle$  after phase discriminator on atoms 1, 2, and 3, then  $|\Psi_4^{00}\rangle$  will become  $|\Psi_3^{00}\rangle$  after phase discriminator on atoms 3, 4, and 1, so we need  $I^1 \otimes \sigma_z^2 \otimes \sigma_z^3 \otimes I^4$  to restore  $|\Psi_3^{00}\rangle$  to  $|\Psi_2^{00}\rangle$ . We list the distinguishment results and the corresponding local unitary operations in Table III.

For five-qubit cluster state, the distinguishment process is shown in Fig. 3(c). Step (i): we determine the parity information of five-qubit states by using PAD1, PAD2 and PAD3 in Fig. 3(c), distinguishing the state  $|\Psi_i^{\mu\nu\lambda}\rangle$  with specific superscript  $\mu$ ,  $\nu$  and  $\lambda$ , where  $i \in \{1, 2, 3, 4, 5\}$ . Step(ii), we use PHD1 and PHD2 in Fig. 3(c) by observing the double

TABLE II. The corresponding relationship between different initial Bell states and the measurement results of the auxiliary atom.

Initial Bell state	Measurement result	
	PHD	PAD
$ \Psi_0^+\rangle_{12} = \frac{1}{\sqrt{2}}( 00\rangle +  11\rangle)$	$ +\rangle_a$	$ +\rangle_a$
$ \Psi_0^-\rangle_{12} = \frac{1}{\sqrt{2}}( 00\rangle -  11\rangle)$	$ -\rangle_a$	$ +\rangle_a$
$ \Psi_1^+\rangle_{12} = \frac{1}{\sqrt{2}}( 01\rangle +  10\rangle)$	$ +\rangle_a$	$ -\rangle_a$
$ \Psi_1^-\rangle_{12} = \frac{1}{\sqrt{2}}( 01\rangle -  10\rangle)$	$ -\rangle_a$	$ -\rangle_a$

TABLE III. The corresponding relationship between different initial cluster states, auxiliary atom measurement results and local unitary operations.

Initial cluster state	Measurement result				Local unitary operation
	PAD1	PAD2	PHD1	PHD2	
$ \Psi_1^{00}\rangle = \frac{1}{2}( 0000\rangle +  0011\rangle +  1100\rangle -  1111\rangle)$	$ +\rangle_a$	$ +\rangle_a$	$ +\rangle_a$	$ -\rangle_a$	$I^1 \otimes \sigma_z^2 \otimes \sigma_z^3 \otimes I^4$
$ \Psi_2^{00}\rangle = \frac{1}{2}( 0000\rangle +  0011\rangle -  1100\rangle +  1111\rangle)$	$ +\rangle_a$	$ +\rangle_a$	$ -\rangle_a$	$ -\rangle_a$	$I^1 \otimes \sigma_z^2 \otimes \sigma_z^3 \otimes I^4$
$ \Psi_3^{00}\rangle = \frac{1}{2}( 0000\rangle -  0011\rangle +  1100\rangle +  1111\rangle)$	$ +\rangle_a$	$ +\rangle_a$	$ +\rangle_a$	$ +\rangle_a$	$I^1 \otimes \sigma_z^2 \otimes \sigma_z^3 \otimes I^4$
$ \Psi_4^{00}\rangle = \frac{1}{2}( 0000\rangle -  0011\rangle -  1100\rangle -  1111\rangle)$	$ +\rangle_a$	$ +\rangle_a$	$ -\rangle_a$	$ +\rangle_a$	$I^1 \otimes \sigma_z^2 \otimes \sigma_z^3 \otimes I^4$
$ \Psi_1^{01}\rangle = \frac{1}{2}( 0001\rangle +  0010\rangle +  1101\rangle -  1110\rangle)$	$ +\rangle_a$	$ -\rangle_a$	$ +\rangle_a$	$ -\rangle_a$	$I^1 \otimes \sigma_z^2 \otimes \sigma_z^3 \otimes I^4$
$ \Psi_2^{01}\rangle = \frac{1}{2}( 0001\rangle +  0010\rangle -  1101\rangle +  1110\rangle)$	$ +\rangle_a$	$ -\rangle_a$	$ -\rangle_a$	$ -\rangle_a$	$I^1 \otimes \sigma_z^2 \otimes \sigma_z^3 \otimes I^4$
$ \Psi_3^{01}\rangle = \frac{1}{2}( 0001\rangle -  0010\rangle +  1101\rangle +  1110\rangle)$	$ +\rangle_a$	$ -\rangle_a$	$ +\rangle_a$	$ +\rangle_a$	$I^1 \otimes \sigma_z^2 \otimes \sigma_z^3 \otimes I^4$
$ \Psi_4^{01}\rangle = \frac{1}{2}( 0001\rangle -  0010\rangle -  1101\rangle -  1110\rangle)$	$ +\rangle_a$	$ -\rangle_a$	$ -\rangle_a$	$ +\rangle_a$	$I^1 \otimes \sigma_z^2 \otimes \sigma_z^3 \otimes I^4$
$ \Psi_1^{10}\rangle = \frac{1}{2}( 0100\rangle +  0111\rangle +  1000\rangle -  1011\rangle)$	$ -\rangle_a$	$ +\rangle_a$	$ +\rangle_a$	$ -\rangle_a$	$\sigma_z^1 \otimes I^2 \otimes \sigma_z^3 \otimes I^4$
$ \Psi_2^{10}\rangle = \frac{1}{2}( 0100\rangle +  0111\rangle -  1000\rangle +  1011\rangle)$	$ -\rangle_a$	$ +\rangle_a$	$ -\rangle_a$	$ -\rangle_a$	$\sigma_z^1 \otimes I^2 \otimes \sigma_z^3 \otimes I^4$
$ \Psi_3^{10}\rangle = \frac{1}{2}( 0100\rangle -  0111\rangle +  1000\rangle +  1011\rangle)$	$ -\rangle_a$	$ +\rangle_a$	$ +\rangle_a$	$ +\rangle_a$	$\sigma_z^1 \otimes I^2 \otimes \sigma_z^3 \otimes I^4$
$ \Psi_4^{10}\rangle = \frac{1}{2}( 0100\rangle -  0111\rangle -  1000\rangle -  1011\rangle)$	$ -\rangle_a$	$ +\rangle_a$	$ -\rangle_a$	$ +\rangle_a$	$\sigma_z^1 \otimes I^2 \otimes \sigma_z^3 \otimes I^4$
$ \Psi_1^{11}\rangle = \frac{1}{2}( 0101\rangle +  0110\rangle +  1001\rangle -  1010\rangle)$	$ -\rangle_a$	$ -\rangle_a$	$ +\rangle_a$	$ -\rangle_a$	$\sigma_z^1 \otimes I^2 \otimes \sigma_z^3 \otimes I^4$
$ \Psi_2^{11}\rangle = \frac{1}{2}( 0101\rangle +  0110\rangle -  1001\rangle +  1010\rangle)$	$ -\rangle_a$	$ -\rangle_a$	$ -\rangle_a$	$ -\rangle_a$	$\sigma_z^1 \otimes I^2 \otimes \sigma_z^3 \otimes I^4$
$ \Psi_3^{11}\rangle = \frac{1}{2}( 0101\rangle -  0110\rangle +  1001\rangle +  1010\rangle)$	$ -\rangle_a$	$ -\rangle_a$	$ +\rangle_a$	$ +\rangle_a$	$\sigma_z^1 \otimes I^2 \otimes \sigma_z^3 \otimes I^4$
$ \Psi_4^{11}\rangle = \frac{1}{2}( 0101\rangle -  0110\rangle -  1001\rangle -  1010\rangle)$	$ -\rangle_a$	$ -\rangle_a$	$ -\rangle_a$	$ +\rangle_a$	$\sigma_z^1 \otimes I^2 \otimes \sigma_z^3 \otimes I^4$

measurement results of the auxiliary atom in Sec. III C to identify the phase information of five-qubit cluster states, distinguishing the state with specific value of subscript  $i$ . Combined with the steps (i) and (ii), the five-qubit cluster states can be distinguished completely and nondestructively. We list the results of the distinguishment in Table IV of Appendix C. There are also many practical applications of the proposed discriminators. Here, we only make a brief discussion for two of them, i.e., quantum teleportation and quantum dense coding, in Appendix D.

V. DISCUSSION AND CONCLUSION

We now discuss the performance and experimental feasibility of the scheme. The entanglement discriminator is employed to distinguish the mixed state practically. Therefore, we set the mixed state to be distinguished as  $\rho(0) = \sum_i P_i \rho_i$ , where  $\rho_i$  is the density matrix of the  $i$ th purity state to be distinguished,  $P_i$  denotes the probability of the state that makes up  $\rho_i$  and  $\sum_i P_i = 1$ ,  $i = 1, 2, 3, \dots, 2^N$ .  $N$  is the qubit number. Finally, all the entangled states are completely distinguished based on the measurement results. Thus, we set the ideal state, after entanglement discriminator is applied, as  $\rho_{ideal} = \rho_i$ . The evolution of the system under consideration of atomic spontaneous emission from Rydberg states to ground states is governed by the Lindblad master equation

$$\dot{\rho}(t) = i[\rho(t), H(t)] + \sum_j \sum_k [L_j^k \rho L_j^{k\dagger} - \frac{1}{2}(L_j^{k\dagger} L_j^k \rho + \rho L_j^{k\dagger} L_j^k)], \tag{16}$$

where  $H(t)$  is the total Hamiltonian,  $\rho(t)$  the density operator of systematic state, and  $L_j^k = \sqrt{\Gamma/2}|k\rangle_j \langle r|$  a Lindblad operator with the superscript  $j$  labeling the  $j$ th atom. The fidelity

is defined as  $F = \text{tr}[\rho(t)\rho_{ideal}]/P_i$ , where  $\rho(t)$  is the evolution density matrix calculated by the master equation in Eq. (16). To evaluate the performance of the quantum logic gate, we use the fidelity definition  $F = |\langle \psi_{ideal} | \psi(t) \rangle|^2$ , where  $|\psi(t)\rangle$  is the state calculated by master equation in Eq. (16) with the given initial state and  $|\psi_{ideal}\rangle$  being the state experiencing the ideal gate.

For the given Rydberg states  $|r\rangle_c = |r\rangle_t = |71s_{1/2}\rangle$ , the RRI strength is  $V = 2\pi \times 185.83$  MHz when the interatomic distance is set about  $d = 4.2 \mu\text{m}$  [92]. The decay rate from Rydberg state  $|r\rangle$  to ground states  $|0\rangle$  and  $|1\rangle$  is about  $\Gamma = 2.5$  kHz [93]. If we choose Eq. (9) as the initial state to evaluate the performance of the proposed CPG in Sec. II B. After solving the master equation numerically, one can get the fidelity versus the Rabi frequency  $\Omega$ , as shown in Fig. 4. In the case of  $\Omega = 2\pi \times 4.67$  MHz, the fidelity can reach 99.84%. When the value of  $\Omega$  is less than  $2\pi \times 4.67$  MHz, however, the evolution time of the system increases, thus the influence of decoherence is enhanced, leading to lower fidelity. While

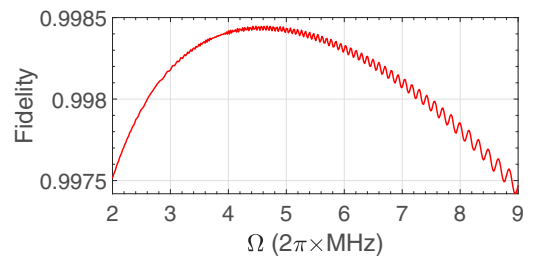


FIG. 4. Performances of different values of  $\Omega$ . The optimal  $\Omega$  is  $2\pi \times 4.67$  MHz, the corresponding fidelity of numerical simulation can reach 99.84%. If  $\Omega/2\pi < 4.67$  MHz, the fidelity is low in virtue of the influence of decoherence with long time. While  $\Omega/2\pi > 4.67$  MHz, fidelity is still low due to blockade errors.

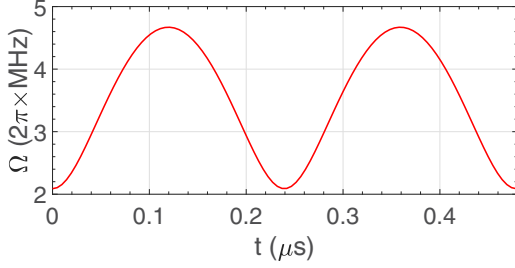


FIG. 5. Schematic diagram of the effective Rabi frequency within a single step time. Maximum value of the Rabi frequency is  $\Omega_{\text{MAX}}/2\pi = 4.67$  MHz.

when the value of  $\Omega$  is greater than  $2\pi \times 4.67$  MHz, the blockade errors enlarge and the fidelity would also decrease. In order to minimize these two kinds of effects, we choose the maximum value of the effective Rabi frequency  $\Omega_{\text{max}} = 2\pi \times 4.67$  MHz, the corresponding time of evolution within a single step is about  $0.49 \mu\text{s}$  and the effective Rabi frequency within a single step time is plotted in Fig. 5.

One can simulate the fidelity of our proposed discriminators with a few qubits. However, it will be challenging when more than four qubits are involved, due to requirement of large size of the density matrix (more than  $3^5 \times 3^5$ ) with respect to the limited computational resource. Here we make a simple estimation to roughly analyze the fidelity of multiqubit discriminators. Our approach is divided into three steps. Step (i): finding the rule. Perform the two-qubit CPG/CNOT gate successively on the system with a group of given initial states, finding out the rule of fidelity versus performance time. Here we only consider the exponential fitting (EF) and linear fitting (LF). Step (ii): validity testing. For a few-body discriminator that can be numerically simulated by solving the master equation, we here also consider the rule in step (i) in the calculation of the fidelity based on the number of CPG and CNOT, and compare these fidelities to test validity of the rule in step (i). Step (iii): estimating fidelity. Estimate the fidelity of many-body entanglement discriminators which is hard to achieve through numerically solving the master equation.

These three steps can be described in detail as follows. Step (i) For two-qubit CNOT gate, with the initial state as  $|\psi\rangle = |00\rangle_{12}$ , we perform this gate  $\mathcal{M}$  times successively and record the fidelity after performing each CNOT gate. We use the fidelity of the CNOT gate for LF, i.e.,  $1 - N \times (1 - F_1)$  and for EF, i.e.,  $(F_1)^N$ , respectively, where  $F_1$  is the fidelity of the CNOT gate. The results are presented in Fig. 6(a). For two-qubit CPG with the initial state  $|\psi\rangle = (|00\rangle_{12} + |01\rangle_{12})/\sqrt{2}$ , the similar results are shown in Fig. 6(b). Finally, we can find that EF agrees with the result of numerical analysis (NA) better than that of LF.

Step (ii): To verify the feasibility of EF, we compare the numerical results of Bell state, three- and four-qubit GHZ-state as well as four-qubit cluster-state discriminators with the results from EF. Suppose that  $m$  CPGs and  $n$  CNOT gates are involved in an entanglement discriminator, the estimated fidelity is given by  $(F_1^{\text{CNOT}})^m \times (F_1^{\text{CPG}})^n$ . Here,  $F_1^{\text{CNOT}}$  and  $F_1^{\text{CPG}}$  denote the gate fidelities of CNOT and CPG, respectively. For example, for the Bell state discriminator, two CPGs and

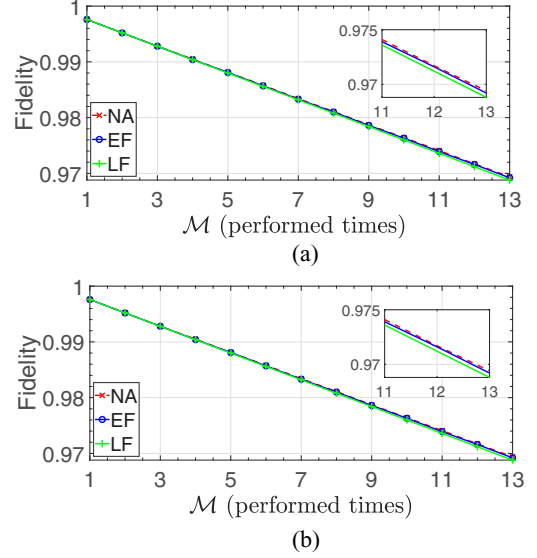


FIG. 6. Schematic diagrams of the comparison among numerical analysis (NA), linear fitting (LF) and exponential fitting (EF) to explore performance of (a) CNOT gate and (b) CPG gate with the initial state in Eq. (9). For (a)  $\alpha = 1$  and  $\beta = \gamma = \delta = 0$ . For (b)  $\alpha = \beta = 1/\sqrt{2}$  and  $\gamma = \delta = 0$  with decay rate  $\Gamma = 2.5$  kHz.

two CNOT gates are used, thus the estimated fidelity should be  $(F_1^{\text{CNOT}})^2 \times (F_1^{\text{CPG}})^2$ . One can calculate that of many-body entanglement discriminator in the similar way. In Table V, we exemplify some cases to test the validity of our thought. One can see that the results of Bell-, GHZ- and cluster-state discriminators from EF and NA are very close to each other.

Step (iii) Following the results from steps (i) and (ii), we are able to fit the fidelity of the many-body entanglement discriminators. Then, we demonstrate the EF results of Bell-state,  $N$ -qubit GHZ-state and cluster-state discriminators in Fig. 7. Besides, we also plot the fidelity of few-body entanglement discriminator achieved by NA. The results show good agreement between EF and NA as well as high fidelity under the consideration of dissipation. It should be noted that throughout our discussion about decoherence, we only considered the decay of Rydberg states. Experimentally, because the auxiliary atoms should be moved or re-trapped when we add individually addressable atomic qubits during

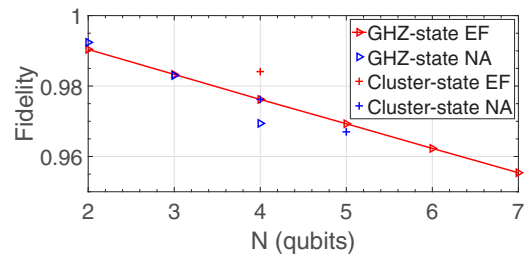


FIG. 7. Schematic diagram of EF of discriminators for Bell state  $|\Psi_0^+\rangle_{12}$ ,  $N$ -qubit GHZ state  $|\Psi_0^+\rangle_{12\dots N}$ , four-qubit cluster state  $|\Psi_3^{00}\rangle$  and five-qubit cluster state  $|\Psi_1^{000}\rangle$  and NA that we can achieve, in which we set decay rate  $\Gamma = 2.5$  kHz. In fact, the two-qubit GHZ state here means the Bell state.



the state discrimination process, the additional source of decoherence would definitely occur. Thus with the consideration of both the Rydberg state decay and the additional decoherence source, the experimental fidelity as well as the scalability of the proposed scheme would be further reduced. In conclusion, we have proposed schemes to achieve many-body entanglement discriminators for  $N$ -qubit GHZ state, four- and five-qubit cluster states as well as two-body Bell state, based on the geometric quantum gate constructed by user-defined passage. To clarify the potential application of entanglement discriminators in quantum information processing, we have exemplified some key operations in quantum teleportation and quantum dense coding. Our numerical simulations have indicated that our proposal works with high fidelity even when  $N = 7$  involving the decay of Rydberg states. In addition, our scheme, based on geometric phases, is robust against the systematic errors. Moreover, our proposed discriminators can

be straightforwardly applied to other three-level systems that are able to construct two-qubit quantum logic gates. Therefore we believe that with further development of quantum technology, our study may be very useful in accomplishing tasks for Rydberg-atom-based quantum information processing in the near future.

### ACKNOWLEDGMENTS

We would like to thank Bao-Jie Liu for useful discussions. This work was supported by the National Natural Science Foundation of China (NSFC) under Grants No. 11804308, No. 11835011, No. 11804375, No. 11734018, and No. 11674360, China Postdoctoral Science Foundation (CPSF) under Grant No. 2018T110735, and Key Research and Development Project of Guangdong Province under Grant No. 2020B0303300001.

### APPENDIX A: SPECIAL RYDBERG DISCRIMINATOR

$$\begin{aligned}
|\Psi^+\rangle \otimes \frac{1}{\sqrt{2}}(|0\rangle_a + |1\rangle_a) &= \frac{1}{\sqrt{2}}[\alpha(|\mu_1 \cdots \mu_N\rangle + |\bar{\mu}_1 \cdots \bar{\mu}_N\rangle) \pm \beta(|v_1 \cdots v_N\rangle + |\bar{v}_1 \cdots \bar{v}_N\rangle)] \otimes (|0\rangle_a + |1\rangle_a) \\
&\xrightarrow{\hat{U}_{cNOT}^N, \dots, \hat{U}_{cNOT}^1} \frac{1}{\sqrt{2}}[\alpha(|\bar{\mu}_1 \cdots \bar{\mu}_N\rangle + |\mu_1 \cdots \mu_N\rangle) \pm \beta(|\bar{v}_1 \cdots \bar{v}_N\rangle + |v_1 \cdots v_N\rangle)] \otimes |0\rangle_a \\
&\quad + \frac{1}{\sqrt{2}}[\alpha(|\mu_1 \cdots \mu_N\rangle + |\bar{\mu}_1 \cdots \bar{\mu}_N\rangle) \pm \beta(|v_1 \cdots v_N\rangle + |\bar{v}_1 \cdots \bar{v}_N\rangle)] \otimes |1\rangle_a \\
&= |\Psi^+\rangle \otimes \frac{1}{\sqrt{2}}(|0\rangle_a + |1\rangle_a), \\
|\Psi^-\rangle \otimes \frac{1}{\sqrt{2}}(|0\rangle_a + |1\rangle_a) &= \frac{1}{\sqrt{2}}[\alpha(|\mu_1 \cdots \mu_N\rangle - |\bar{\mu}_1 \cdots \bar{\mu}_N\rangle) \pm \beta(|v_1 \cdots v_N\rangle - |\bar{v}_1 \cdots \bar{v}_N\rangle)] \otimes (|0\rangle_a + |1\rangle_a) \\
&\xrightarrow{\hat{U}_{cNOT}^N, \dots, \hat{U}_{cNOT}^1} \frac{1}{\sqrt{2}}[\alpha(|\bar{\mu}_1 \cdots \bar{\mu}_N\rangle - |\mu_1 \cdots \mu_N\rangle) \pm \beta(|\bar{v}_1 \cdots \bar{v}_N\rangle - |v_1 \cdots v_N\rangle)] \otimes |0\rangle_a \\
&\quad + \frac{1}{\sqrt{2}}[\alpha(|\mu_1 \cdots \mu_N\rangle - |\bar{\mu}_1 \cdots \bar{\mu}_N\rangle) \pm \beta(|v_1 \cdots v_N\rangle - |\bar{v}_1 \cdots \bar{v}_N\rangle)] \otimes |1\rangle_a \\
&= |\Psi^-\rangle \otimes \frac{1}{\sqrt{2}}(|1\rangle_a - |0\rangle_a). \tag{A1}
\end{aligned}$$

This discriminator has special ability to distinguish  $|\Psi^+\rangle$  and  $|\Psi^-\rangle$ . Both GHZ-state and five-qubit cluster-state phase discriminators can be regarded as its special cases.

### APPENDIX B: FOUR-QUBIT CLUSTER-STATE PHASE DISCRIMINATOR

$$\begin{aligned}
|\Psi_1^{\mu\nu}\rangle \otimes \frac{1}{\sqrt{2}}(|0\rangle_a + |1\rangle_a) &= \frac{1}{2\sqrt{2}}(|0\mu 0\nu\rangle + |0\mu 1\bar{\nu}\rangle + |1\bar{\mu} 0\nu\rangle - |1\bar{\mu} 1\bar{\nu}\rangle) \otimes (|0\rangle_a + |1\rangle_a) \\
&\xrightarrow{\hat{U}_{cNOT}^2, \hat{U}_{cNOT}^1} \frac{1}{2\sqrt{2}}[(|1\bar{\mu} 0\nu\rangle + |1\bar{\mu} 1\bar{\nu}\rangle + |0\mu 0\nu\rangle - |0\mu 1\bar{\nu}\rangle) \otimes |0\rangle_a + (|0\mu 0\nu\rangle + |0\mu 1\bar{\nu}\rangle) \\
&\quad + |1\bar{\mu} 0\nu\rangle - |1\bar{\mu} 1\bar{\nu}\rangle) \otimes |1\rangle_a] \\
&\xrightarrow{\hat{U}_{CPG}^3} \frac{1}{2\sqrt{2}}[(|1\bar{\mu} 0\nu\rangle + |1\bar{\mu} 1\bar{\nu}\rangle + |0\mu 0\nu\rangle - |0\mu 1\bar{\nu}\rangle) \otimes |0\rangle_a + (|0\mu 0\nu\rangle - |0\mu 1\bar{\nu}\rangle + |1\bar{\mu} 0\nu\rangle \\
&\quad + |1\bar{\mu} 1\bar{\nu}\rangle) \otimes |1\rangle_a] \\
&= |\Psi_3^{\mu\nu}\rangle \otimes \frac{1}{\sqrt{2}}(|0\rangle_a + |1\rangle_a),
\end{aligned}$$

$$\begin{aligned}
|\Psi_2^{\mu\nu}\rangle \otimes \frac{1}{\sqrt{2}}(|0\rangle_a + |1\rangle_a) &= \frac{1}{2\sqrt{2}}(|0\mu 0\nu\rangle + |0\mu 1\bar{\nu}\rangle - |1\bar{\mu} 0\nu\rangle + |1\bar{\mu} 1\bar{\nu}\rangle) \otimes (|0\rangle_a + |1\rangle_a) \\
&\xrightarrow{\hat{U}_{CNOT}^2 \hat{U}_{CNOT}^1} \frac{1}{2\sqrt{2}}[(|1\bar{\mu} 0\nu\rangle + |1\bar{\mu} 1\bar{\nu}\rangle - |0\mu 0\nu\rangle + |0\mu 1\bar{\nu}\rangle) \otimes |0\rangle_a + (|0\mu 0\nu\rangle + |0\mu 1\bar{\nu}\rangle - |1\bar{\mu} 0\nu\rangle \\
&\quad + |1\bar{\mu} 1\bar{\nu}\rangle) \otimes |1\rangle_a] \\
&\xrightarrow{\hat{U}_{CPG}^3} \frac{1}{2\sqrt{2}}[(|1\bar{\mu} 0\nu\rangle + |1\bar{\mu} 1\bar{\nu}\rangle - |0\mu 0\nu\rangle + |0\mu 1\bar{\nu}\rangle) \otimes |0\rangle_a + (|0\mu 0\nu\rangle - |0\mu 1\bar{\nu}\rangle - |1\bar{\mu} 0\nu\rangle \\
&\quad - |1\bar{\mu} 1\bar{\nu}\rangle) \otimes |1\rangle_a] \\
&= |\Psi_4^{\mu\nu}\rangle \otimes \frac{1}{\sqrt{2}}(|1\rangle_a - |0\rangle_a), \\
|\Psi_1^{\mu\nu}\rangle \otimes \frac{1}{\sqrt{2}}(|0\rangle_a + |1\rangle_a) &= \frac{1}{2\sqrt{2}}(|0\mu 0\nu\rangle + |0\mu 1\bar{\nu}\rangle + |1\bar{\mu} 0\nu\rangle - |1\bar{\mu} 1\bar{\nu}\rangle) \otimes (|0\rangle_a + |1\rangle_a) \\
&\xrightarrow{\hat{U}_{CNOT}^4 \hat{U}_{CNOT}^3} \frac{1}{2\sqrt{2}}[(|0\mu 1\bar{\nu}\rangle + |0\mu 0\nu\rangle + |1\bar{\mu} 1\bar{\nu}\rangle - |1\bar{\mu} 0\nu\rangle) \otimes |0\rangle_a + (|0\mu 0\nu\rangle + |0\mu 1\bar{\nu}\rangle + |1\bar{\mu} 0\nu\rangle \\
&\quad - |1\bar{\mu} 1\bar{\nu}\rangle) \otimes |1\rangle_a] \\
&\xrightarrow{\hat{U}_{CPG}^1} \frac{1}{2\sqrt{2}}[(|0\mu 1\bar{\nu}\rangle + |0\mu 0\nu\rangle + |1\bar{\mu} 1\bar{\nu}\rangle - |1\bar{\mu} 0\nu\rangle) \otimes |0\rangle_a + (|0\mu 0\nu\rangle + |0\mu 1\bar{\nu}\rangle - |1\bar{\mu} 0\nu\rangle \\
&\quad + |1\bar{\mu} 1\bar{\nu}\rangle) \otimes |1\rangle_a] \\
&= |\Psi_2^{\mu\nu}\rangle \otimes \frac{1}{\sqrt{2}}(|0\rangle_a + |1\rangle_a), \\
|\Psi_3^{\mu\nu}\rangle \otimes \frac{1}{\sqrt{2}}(|0\rangle_a + |1\rangle_a) &= \frac{1}{2\sqrt{2}}(|0\mu 0\nu\rangle - |0\mu 1\bar{\nu}\rangle + |1\bar{\mu} 0\nu\rangle + |1\bar{\mu} 1\bar{\nu}\rangle) \otimes (|0\rangle_a + |1\rangle_a) \\
&\xrightarrow{\hat{U}_{CNOT}^4 \hat{U}_{CNOT}^3} \frac{1}{2\sqrt{2}}[(|0\mu 1\bar{\nu}\rangle - |0\mu 0\nu\rangle + |1\bar{\mu} 1\bar{\nu}\rangle + |1\bar{\mu} 0\nu\rangle) \otimes |0\rangle_a + (|0\mu 0\nu\rangle - |0\mu 1\bar{\nu}\rangle + |1\bar{\mu} 0\nu\rangle \\
&\quad + |1\bar{\mu} 1\bar{\nu}\rangle) \otimes |1\rangle_a] \\
&\xrightarrow{\hat{U}_{CPG}^1} \frac{1}{2\sqrt{2}}[(|0\mu 1\bar{\nu}\rangle - |0\mu 0\nu\rangle + |1\bar{\mu} 1\bar{\nu}\rangle + |1\bar{\mu} 0\nu\rangle) \otimes |0\rangle_a + (|0\mu 0\nu\rangle - |0\mu 1\bar{\nu}\rangle - |1\bar{\mu} 0\nu\rangle \\
&\quad - |1\bar{\mu} 1\bar{\nu}\rangle) \otimes |1\rangle_a] \\
&= |\Psi_4^{\mu\nu}\rangle \otimes \frac{1}{\sqrt{2}}(|1\rangle_a - |0\rangle_a). \tag{B1}
\end{aligned}$$

### APPENDIX C: FIVE-QUBIT CLUSTER-STATE RYDBERG DISCRIMINATOR

For five-qubit cluster-state discriminators, each cluster state would be distinguished completely and nondestructively. We list the each cluster state and the corresponding result of the distinguishment in Table IV.

TABLE IV. The corresponding relationship between different initial cluster states and the measurement results of the auxiliary atom. Here for three-qubit state  $|000\rangle_{jkm}$ ,  $|011\rangle_{jkm}$ ,  $|101\rangle_{jkm}$ ,  $|110\rangle_{jkm}$ , the measurement result of the auxiliary atom is  $|+\rangle_a$ , implying even parity, while for three-qubit state  $|001\rangle_{jkm}$ ,  $|010\rangle_{jkm}$ ,  $|100\rangle_{jkm}$ ,  $|111\rangle_{jkm}$ , the measurement result is  $|-\rangle_a$ , implying odd parity, which correspond to the results of PAD2 when  $j$ ,  $k$ , and  $m$  are 2, 3, and 4, respectively, while correspond to the results of PAD3 when  $j$ ,  $k$ , and  $m$  are 2, 4, and 5, respectively.

Initial cluster state	Measurement result				
	PAD1	PAD2	PAD3	PHD1	PHD2
$ \Psi_1^{000}\rangle = \frac{1}{2}( 00000\rangle +  00111\rangle +  11101\rangle +  11010\rangle)$	$ +\rangle_a$	$ +\rangle_a$	$ +\rangle_a$	$ +\rangle_a$	$ +\rangle_a$
$ \Psi_2^{000}\rangle = \frac{1}{2}( 00000\rangle -  00111\rangle +  11101\rangle -  11010\rangle)$	$ +\rangle_a$	$ +\rangle_a$	$ +\rangle_a$	$ -\rangle_a$	$ -\rangle_a$
$ \Psi_3^{000}\rangle = \frac{1}{2}( 00000\rangle +  00111\rangle -  11101\rangle -  11010\rangle)$	$ +\rangle_a$	$ +\rangle_a$	$ +\rangle_a$	$ +\rangle_a$	$ -\rangle_a$
$ \Psi_4^{000}\rangle = \frac{1}{2}( 00000\rangle -  00111\rangle -  11101\rangle +  11010\rangle)$	$ +\rangle_a$	$ +\rangle_a$	$ +\rangle_a$	$ -\rangle_a$	$ +\rangle_a$
$ \Psi_1^{001}\rangle = \frac{1}{2}( 00001\rangle +  00110\rangle +  11100\rangle +  11011\rangle)$	$ +\rangle_a$	$ +\rangle_a$	$ -\rangle_a$	$ +\rangle_a$	$ +\rangle_a$
$ \Psi_2^{001}\rangle = \frac{1}{2}( 00001\rangle -  00110\rangle +  11100\rangle -  11011\rangle)$	$ +\rangle_a$	$ +\rangle_a$	$ -\rangle_a$	$ -\rangle_a$	$ -\rangle_a$
$ \Psi_3^{001}\rangle = \frac{1}{2}( 00001\rangle +  00110\rangle -  11100\rangle -  11011\rangle)$	$ +\rangle_a$	$ +\rangle_a$	$ -\rangle_a$	$ +\rangle_a$	$ -\rangle_a$
$ \Psi_4^{001}\rangle = \frac{1}{2}( 00001\rangle -  00110\rangle -  11100\rangle +  11011\rangle)$	$ +\rangle_a$	$ +\rangle_a$	$ -\rangle_a$	$ -\rangle_a$	$ +\rangle_a$
$ \Psi_1^{010}\rangle = \frac{1}{2}( 00010\rangle +  00101\rangle +  11111\rangle +  11000\rangle)$	$ +\rangle_a$	$ -\rangle_a$	$ -\rangle_a$	$ +\rangle_a$	$ +\rangle_a$
$ \Psi_2^{010}\rangle = \frac{1}{2}( 00010\rangle -  00101\rangle +  11111\rangle -  11000\rangle)$	$ +\rangle_a$	$ -\rangle_a$	$ -\rangle_a$	$ -\rangle_a$	$ -\rangle_a$
$ \Psi_3^{010}\rangle = \frac{1}{2}( 00010\rangle +  00101\rangle -  11111\rangle -  11000\rangle)$	$ +\rangle_a$	$ -\rangle_a$	$ -\rangle_a$	$ +\rangle_a$	$ -\rangle_a$
$ \Psi_4^{010}\rangle = \frac{1}{2}( 00010\rangle -  00101\rangle -  11111\rangle +  11000\rangle)$	$ +\rangle_a$	$ -\rangle_a$	$ -\rangle_a$	$ -\rangle_a$	$ +\rangle_a$
$ \Psi_1^{011}\rangle = \frac{1}{2}( 00011\rangle +  00100\rangle +  11110\rangle +  11001\rangle)$	$ +\rangle_a$	$ -\rangle_a$	$ +\rangle_a$	$ +\rangle_a$	$ +\rangle_a$
$ \Psi_2^{011}\rangle = \frac{1}{2}( 00011\rangle -  00100\rangle +  11110\rangle -  11001\rangle)$	$ +\rangle_a$	$ -\rangle_a$	$ +\rangle_a$	$ -\rangle_a$	$ -\rangle_a$
$ \Psi_3^{011}\rangle = \frac{1}{2}( 00011\rangle +  00100\rangle -  11110\rangle -  11001\rangle)$	$ +\rangle_a$	$ -\rangle_a$	$ +\rangle_a$	$ +\rangle_a$	$ -\rangle_a$
$ \Psi_4^{011}\rangle = \frac{1}{2}( 00011\rangle -  00100\rangle -  11110\rangle +  11001\rangle)$	$ +\rangle_a$	$ -\rangle_a$	$ +\rangle_a$	$ -\rangle_a$	$ +\rangle_a$
$ \Psi_1^{100}\rangle = \frac{1}{2}( 01000\rangle +  01111\rangle +  10101\rangle +  10010\rangle)$	$ -\rangle_a$	$ -\rangle_a$	$ -\rangle_a$	$ +\rangle_a$	$ +\rangle_a$
$ \Psi_2^{100}\rangle = \frac{1}{2}( 01000\rangle -  01111\rangle +  10101\rangle -  10010\rangle)$	$ -\rangle_a$	$ -\rangle_a$	$ -\rangle_a$	$ -\rangle_a$	$ -\rangle_a$
$ \Psi_3^{100}\rangle = \frac{1}{2}( 01000\rangle +  01111\rangle -  10101\rangle -  10010\rangle)$	$ -\rangle_a$	$ -\rangle_a$	$ -\rangle_a$	$ +\rangle_a$	$ -\rangle_a$
$ \Psi_4^{100}\rangle = \frac{1}{2}( 01000\rangle -  01111\rangle -  10101\rangle +  10010\rangle)$	$ -\rangle_a$	$ -\rangle_a$	$ -\rangle_a$	$ -\rangle_a$	$ +\rangle_a$
$ \Psi_1^{101}\rangle = \frac{1}{2}( 01001\rangle +  01110\rangle +  10100\rangle +  10011\rangle)$	$ -\rangle_a$	$ -\rangle_a$	$ +\rangle_a$	$ +\rangle_a$	$ +\rangle_a$
$ \Psi_2^{101}\rangle = \frac{1}{2}( 01001\rangle -  01110\rangle +  10100\rangle -  10011\rangle)$	$ -\rangle_a$	$ -\rangle_a$	$ +\rangle_a$	$ -\rangle_a$	$ -\rangle_a$
$ \Psi_3^{101}\rangle = \frac{1}{2}( 01001\rangle +  01110\rangle -  10100\rangle -  10011\rangle)$	$ -\rangle_a$	$ -\rangle_a$	$ +\rangle_a$	$ +\rangle_a$	$ -\rangle_a$
$ \Psi_4^{101}\rangle = \frac{1}{2}( 01001\rangle -  01110\rangle -  10100\rangle +  10011\rangle)$	$ -\rangle_a$	$ -\rangle_a$	$ +\rangle_a$	$ -\rangle_a$	$ +\rangle_a$
$ \Psi_1^{110}\rangle = \frac{1}{2}( 01010\rangle +  01101\rangle +  10111\rangle +  10000\rangle)$	$ -\rangle_a$	$ +\rangle_a$	$ +\rangle_a$	$ +\rangle_a$	$ +\rangle_a$
$ \Psi_2^{110}\rangle = \frac{1}{2}( 01010\rangle -  01101\rangle +  10111\rangle -  10000\rangle)$	$ -\rangle_a$	$ +\rangle_a$	$ +\rangle_a$	$ -\rangle_a$	$ -\rangle_a$
$ \Psi_3^{110}\rangle = \frac{1}{2}( 01010\rangle +  01101\rangle -  10111\rangle -  10000\rangle)$	$ -\rangle_a$	$ +\rangle_a$	$ +\rangle_a$	$ +\rangle_a$	$ -\rangle_a$
$ \Psi_4^{110}\rangle = \frac{1}{2}( 01010\rangle -  01101\rangle -  10111\rangle +  10000\rangle)$	$ -\rangle_a$	$ +\rangle_a$	$ +\rangle_a$	$ -\rangle_a$	$ +\rangle_a$
$ \Psi_1^{111}\rangle = \frac{1}{2}( 01011\rangle +  01100\rangle +  10110\rangle +  10001\rangle)$	$ -\rangle_a$	$ +\rangle_a$	$ -\rangle_a$	$ +\rangle_a$	$ +\rangle_a$
$ \Psi_2^{111}\rangle = \frac{1}{2}( 01011\rangle -  01100\rangle +  10110\rangle -  10001\rangle)$	$ -\rangle_a$	$ +\rangle_a$	$ -\rangle_a$	$ -\rangle_a$	$ -\rangle_a$
$ \Psi_3^{111}\rangle = \frac{1}{2}( 01011\rangle +  01100\rangle -  10110\rangle -  10001\rangle)$	$ -\rangle_a$	$ +\rangle_a$	$ -\rangle_a$	$ +\rangle_a$	$ -\rangle_a$
$ \Psi_4^{111}\rangle = \frac{1}{2}( 01011\rangle -  01100\rangle -  10110\rangle +  10001\rangle)$	$ -\rangle_a$	$ +\rangle_a$	$ -\rangle_a$	$ -\rangle_a$	$ +\rangle_a$

**APPENDIX D: APPLICATIONS OF ENTANGLEMENT DISCRIMINATOR**

Here we demonstrate applications of our proposed entanglement discriminators in quantum teleportation and quantum dense coding.

TABLE V. Comparison between NA of Bell-state discriminators and EF rule after successive gate operations, in which no effect of local unitary operations on four-qubit cluster states is considered.

Different initial state	NA	EF
$( 00\rangle +  11\rangle)/\sqrt{2}$	99.24%	99.04%
$( 000\rangle +  111\rangle)/\sqrt{2}$	98.30%	98.33%
$( 0000\rangle +  1111\rangle)/\sqrt{2}$	96.94%	97.62%
$( 0000\rangle -  0011\rangle +  1100\rangle +  1111\rangle)/2$	98.41%	97.62%

**1. Quantum teleportation**

Quantum teleportation [88] presents a process in which quantum information can be transmitted from one location to another, with the help of classical communication and previously shared quantum entanglement between the sending and receiving locations. Now, we show how to accomplish teleportation by using our proposed entanglement discriminators. If Alice initially possesses a single atom with

$$|\phi\rangle_1 = c_1|0\rangle_1 + c_2|1\rangle_1,$$

where  $c_1$  and  $c_2$  are unknown coefficients with  $|c_1|^2 + |c_2|^2 = 1$ . If two other atoms 2 and 3 are prepared in entangled Bell state  $|\Psi_1^-\rangle_{23} = \frac{1}{\sqrt{2}}(|01\rangle - |10\rangle)_{23}$ , and the atom 2 is given to Alice, while the atom 3 is given to Bob. Thus the complete

state of the three atom is

$$\begin{aligned}
|\Psi\rangle &= |\phi\rangle_1 |\Psi_1^-\rangle_{23} \\
&= (c_1|0\rangle + c_2|1\rangle)_1 \otimes \frac{1}{\sqrt{2}}(|01\rangle - |10\rangle)_{23} \\
&= \frac{c_1}{\sqrt{2}}(|001\rangle - |010\rangle)_{123} + \frac{c_2}{\sqrt{2}}(|101\rangle - |110\rangle)_{123} \\
&= \frac{1}{2} [ |\Psi_0^+\rangle_{12} (c_1|1\rangle - c_2|0\rangle)_3 + |\Psi_0^-\rangle_{12} (c_1|1\rangle + c_2|0\rangle)_3 \\
&\quad + |\Psi_1^+\rangle_{12} (c_2|1\rangle - c_1|0\rangle)_3 - |\Psi_1^-\rangle_{12} (c_2|1\rangle + c_1|0\rangle)_3 ].
\end{aligned} \tag{D1}$$

where the direct product of atoms 1 and 2 is re-expressed as Bell states. Alice performs Bell-state measurement on atoms 1 and 2 of her own by Bell-state discriminator, and each probability of Bell state is 1/4. After measurement of Alice, the state of atom 3 of Bob will also be determined by Eq. (D1). In order to get the information of initial state of atom 1, Bob only need to perform the corresponding unitary operation to atom 3. For example, if measurement result of Alice is  $|\Psi_0^+\rangle_{12}$ , the corresponding state of the atom 3 is  $(c_1|1\rangle - c_2|0\rangle)_3$  and perform  $\hat{U}_y^3(c_1|1\rangle - c_2|0\rangle)_3 = (c_1|0\rangle + c_2|1\rangle)_3$  to atom 3 to get the same state as atom 1, where  $U_y^3 = i \begin{pmatrix} 0 & -i \\ i & 0 \end{pmatrix}$  is for a Pauli Y gate. Other corresponding states of the atom 3 and unitary operations are  $|\Psi_0^-\rangle_{12} \leftrightarrow \hat{U}_x^3(c_1|1\rangle + c_2|0\rangle)_3$ ,  $|\Psi_1^+\rangle_{12} \leftrightarrow (-\hat{U}_z^3)(c_2|1\rangle - c_1|0\rangle)_3$ ,  $|\Psi_1^-\rangle_{12} \leftrightarrow \hat{U}_I^3(c_2|1\rangle + c_1|0\rangle)_3$ , where  $\hat{U}_I^3 = \begin{pmatrix} 1 & 0 \\ 0 & 1 \end{pmatrix}$  is for a identity quantum gate. Through classical channels, such as telephone, etc., Alice tells Bob the measurement results, and Bob can select the corresponding unitary operation to obtain information of atom 1. Then, quantum teleportation will be realized.

## 2. Quantum dense coding

We discuss below how to accomplish a quantum dense coding [89] using our proposed entanglement discriminators.

TABLE VI. The relationship between local operations by Alice, the new cluster state and the corresponding classical information.

Local operations	Transformed states	Transmitted information
$\hat{U}_I^2 \hat{U}_I^4$	$ \Psi_1^{00}\rangle_{1234}$	0000
$\hat{U}_z^2 \hat{U}_I^4$	$ \Psi_2^{00}\rangle_{1234}$	1000
$\hat{U}_I^2 \hat{U}_z^4$	$ \Psi_3^{00}\rangle_{1234}$	0010
$\hat{U}_z^2 \hat{U}_z^4$	$ \Psi_4^{00}\rangle_{1234}$	1010
$\hat{U}_I^2 \hat{U}_x^4$	$ \Psi_1^{01}\rangle_{1234}$	0001
$\hat{U}_z^2 \hat{U}_x^4$	$ \Psi_2^{01}\rangle_{1234}$	1001
$-\hat{U}_I^2 \hat{U}_y^4$	$ \Psi_3^{01}\rangle_{1234}$	0011
$-\hat{U}_z^2 \hat{U}_y^4$	$ \Psi_4^{01}\rangle_{1234}$	1011
$\hat{U}_x^2 \hat{U}_I^4$	$ \Psi_1^{10}\rangle_{1234}$	0100
$-\hat{U}_y^2 \hat{U}_I^4$	$ \Psi_2^{10}\rangle_{1234}$	1100
$\hat{U}_x^2 \hat{U}_z^4$	$ \Psi_3^{10}\rangle_{1234}$	0110
$-\hat{U}_y^2 \hat{U}_z^4$	$ \Psi_4^{10}\rangle_{1234}$	1110
$\hat{U}_x^2 \hat{U}_x^4$	$ \Psi_1^{11}\rangle_{1234}$	0101
$-\hat{U}_y^2 \hat{U}_x^4$	$ \Psi_2^{11}\rangle_{1234}$	1101
$-\hat{U}_z^2 \hat{U}_x^4$	$ \Psi_3^{11}\rangle_{1234}$	0111
$\hat{U}_y^2 \hat{U}_y^4$	$ \Psi_4^{11}\rangle_{1234}$	1111

The protocol starts with the preparation of a cluster state, i.e.,  $|\Psi_1^{00}\rangle_{1234} = \frac{1}{2}(|0000\rangle + |0011\rangle + |1100\rangle - |1111\rangle)_{1234}$ . The atoms 2 and 4 are sent to Alice and the atoms 1 and 3 are sent to Bob. Alice can perform four possible operations  $\hat{U}_I$ ,  $\hat{U}_x$ ,  $\hat{U}_y$ ,  $\hat{U}_z$  on atom 2 or 4, respectively. We carry out 16 kinds of local operations on two atoms to define four bits of classical information. For example, if Alice wants to send the classical four-bit string 0000 to Bob, she could apply the operation  $\hat{U}_I^2 \hat{U}_I^4$  to atoms 2 and 4, and  $|\Psi_1^{00}\rangle_{1234}$  is unchanged. The other corresponding correlations between local operations and classical information are listed in Table VI. After having performed one of the operations, Alice sends her two atoms to Bob. Then Bob can know what operation Alice performs by using four-qubit cluster-state discriminator to measure the new cluster state, the corresponding classical information that Alice wants to send can be obtained by Bob. In this process, two qubits are sent while four-qubit classical information are transmitted, i.e., quantum dense coding was realized.

- [1] D. Jaksch, J. I. Cirac, P. Zoller, S. L. Rolston, R. Côté, and M. D. Lukin, *Phys. Rev. Lett.* **85**, 2208 (2000).
- [2] M. Saffman, T. G. Walker, and K. Mølmer, *Rev. Mod. Phys.* **82**, 2313 (2010).
- [3] A. Gaëtan, Y. Miroshnychenko, T. Wilk, A. Chotia, M. Viteau, D. Comparat, P. Pillet, A. Browaeys, and P. Grangier, *Nat. Phys.* **5**, 115 (2009).
- [4] M. Saffman, *J. Phys. B: Atom., Mol. Opt. Phys.* **49**, 202001 (2016).
- [5] D. Barredo, S. Ravets, H. Labuhn, L. Béguin, A. Vernier, F. Nogrette, T. Lahaye, and A. Browaeys, *Phys. Rev. Lett.* **112**, 183002 (2014).
- [6] E. Urban, T. A. Johnson, T. Henage, L. Isenhower, D. D. Yavuz, T. G. Walker, and M. Saffman, *Nat. Phys.* **5**, 110 (2009).
- [7] T. F. Gallagher, *Rydberg Atoms*, Vol. 3 (Cambridge University Press, Cambridge, 2005).
- [8] L. Béguin, A. Vernier, R. Chicireanu, T. Lahaye, and A. Browaeys, *Phys. Rev. Lett.* **110**, 263201 (2013).
- [9] X.-F. Shi, *Phys. Rev. Appl.* **7**, 064017 (2017); **10**, 034006 (2018); X.-F. Shi and T. A. B. Kennedy, *Phys. Rev. A* **95**, 043429 (2017); X.-F. Shi, *Phys. Rev. Appl.* **11**, 044035 (2019).
- [10] M. D. Lukin, M. Fleischhauer, R. Cote, L. M. Duan, D. Jaksch, J. I. Cirac, and P. Zoller, *Phys. Rev. Lett.* **87**, 037901 (2001).
- [11] D. Møller, L. B. Madsen, and K. Mølmer, *Phys. Rev. Lett.* **100**, 170504 (2008).
- [12] M. Saffman and K. Mølmer, *Phys. Rev. Lett.* **102**, 240502 (2009).
- [13] L. Isenhower, E. Urban, X. L. Zhang, A. T. Gill, T. Henage, T. A. Johnson, T. G. Walker, and M. Saffman, *Phys. Rev. Lett.* **104**, 010503 (2010).
- [14] X. L. Zhang, L. Isenhower, A. T. Gill, T. G. Walker, and M. Saffman, *Phys. Rev. A* **82**, 030306(R) (2010).

- [15] T. Wilk, A. Gaëtan, C. Evellin, J. Wolters, Y. Miroshnychenko, P. Grangier, and A. Browaeys, *Phys. Rev. Lett.* **104**, 010502 (2010).
- [16] K. M. Maller, M. T. Lichtman, T. Xia, Y. Sun, M. J. Piotrowicz, A. W. Carr, L. Isenhower, and M. Saffman, *Phys. Rev. A* **92**, 022336 (2015).
- [17] Y. Zeng, P. Xu, X. He, Y. Liu, M. Liu, J. Wang, D. J. Papoular, G. V. Shlyapnikov, and M. Zhan, *Phys. Rev. Lett.* **119**, 160502 (2017).
- [18] C. J. Picken, R. Legaie, K. McDonnell, and J. D. Pritchard, *Quantum Sci. Technol.* **4**, 015011 (2018).
- [19] H. Levine, A. Keesling, G. Semeghini, A. Omran, T. T. Wang, S. Ebadi, H. Bernien, M. Greiner, V. Vuletić, H. Pichler, and M. D. Lukin, *Phys. Rev. Lett.* **123**, 170503 (2019).
- [20] H. Levine, A. Keesling, A. Omran, H. Bernien, S. Schwartz, A. S. Zibrov, M. Endres, M. Greiner, V. Vuletić, and M. D. Lukin, *Phys. Rev. Lett.* **121**, 123603 (2018).
- [21] T. M. Graham, M. Kwon, B. Grinkemeyer, Z. Marra, X. Jiang, M. T. Lichtman, Y. Sun, M. Ebert, and M. Saffman, *Phys. Rev. Lett.* **123**, 230501 (2019).
- [22] I. S. Madjarov, J. P. Covey, A. L. Shaw, J. Choi, A. Kale, A. Cooper, H. Pichler, V. Schkolnik, J. R. Williams, and M. Endres, *Nat. Phys.* **16**, 857 (2020).
- [23] D. Petrosyan, F. Motzoi, M. Saffman, and K. Mølmer, *Phys. Rev. A* **96**, 042306 (2017).
- [24] I. I. Beterov, I. N. Ashkarin, E. A. Yakshina, D. B. Tretyakov, V. M. Entin, I. I. Ryabtsev, P. Cheinet, P. Pillet, and M. Saffman, *Phys. Rev. A* **98**, 042704 (2018).
- [25] I. I. Beterov, G. N. Hamzina, E. A. Yakshina, D. B. Tretyakov, V. M. Entin, and I. I. Ryabtsev, *Phys. Rev. A* **97**, 032701 (2018).
- [26] A. Mitra, M. J. Martin, G. W. Biedermann, A. M. Marino, P. M. Poggi, and I. H. Deutsch, *Phys. Rev. A* **101**, 030301(R) (2020).
- [27] M. Khazali and K. Mølmer, *Phys. Rev. X* **10**, 021054 (2020).
- [28] J. T. Young, P. Bienias, R. Belyansky, A. M. Kaufman, and A. V. Gorshkov, [arXiv:2006.02486](https://arxiv.org/abs/2006.02486).
- [29] C.-Y. Guo, L.-L. Yan, S. Zhang, S.-L. Su, and W. Li, *Phys. Rev. A* **102**, 042607 (2020).
- [30] M. Saffman, I. I. Beterov, A. Dalal, E. J. Páez, and B. C. Sanders, *Phys. Rev. A* **101**, 062309 (2020).
- [31] C. Ates, T. Pohl, T. Pattard, and J. M. Rost, *Phys. Rev. Lett.* **98**, 023002 (2007).
- [32] A. W. Carr and M. Saffman, *Phys. Rev. Lett.* **111**, 033607 (2013).
- [33] S.-L. Su, Y. Tian, H. Z. Shen, H. Zang, E. Liang, and S. Zhang, *Phys. Rev. A* **96**, 042335 (2017); S.-L. Su, Y. Gao, E. Liang, and S. Zhang, *ibid.* **95**, 022319 (2017); S. L. Su, H. Z. Shen, E. Liang, and S. Zhang, *ibid.* **98**, 032306 (2018).
- [34] D. Petrosyan and K. Mølmer, *Phys. Rev. Lett.* **113**, 123003 (2014).
- [35] D. X. Li and X. Q. Shao, *Phys. Rev. A* **98**, 062338 (2018).
- [36] P. P. Mazza, R. Schmidt, and I. Lesanovsky, *Phys. Rev. Lett.* **125**, 033602 (2020).
- [37] F. M. Gambetta, W. Li, F. Schmidt-Kaler, and I. Lesanovsky, *Phys. Rev. Lett.* **124**, 043402 (2020).
- [38] F. M. Gambetta, C. Zhang, M. Hennrich, I. Lesanovsky, and W. Li, *Phys. Rev. Lett.* **125**, 133602 (2020).
- [39] I. Bouchoule and K. Mølmer, *Phys. Rev. A* **65**, 041803(R) (2002).
- [40] J. E. Johnson and S. L. Rolston, *Phys. Rev. A* **82**, 033412 (2010).
- [41] G. Pupillo, A. Micheli, M. Boninsegni, I. Lesanovsky, and P. Zoller, *Phys. Rev. Lett.* **104**, 223002 (2010).
- [42] R. Horodecki, P. Horodecki, M. Horodecki, and K. Horodecki, *Rev. Mod. Phys.* **81**, 865 (2009).
- [43] J.-W. Pan, Z.-B. Chen, C.-Y. Lu, H. Weinfurter, A. Zeilinger, and M. Żukowski, *Rev. Mod. Phys.* **84**, 777 (2012).
- [44] D. M. Greenberger, M. A. Horne, and A. Zeilinger, in *Bell's Theorem, Quantum Theory and Conceptions of the Universe*, Fundamental Theories of Physics, Vol. 37, edited by M. Kafatos (Springer, Dordrecht, 1989), pp. 69–72.
- [45] S. Schauer, M. Huber, and B. C. Hiesmayr, *Phys. Rev. A* **82**, 062311 (2010).
- [46] A. Farouk, J. Batle, M. Elhoseny, M. Naseri, M. Lone, A. Fedorov, M. Alkhambashi, S. H. Ahmed, and M. Abdel-Aty, *Front. Phys.* **13**, 130306 (2017).
- [47] V. Giovannetti, S. Lloyd, and L. Maccone, *Science* **306**, 1330 (2004).
- [48] T. Tanamoto, Y.-x. Liu, X. Hu, and F. Nori, *Phys. Rev. Lett.* **102**, 100501 (2009).
- [49] J. Q. You, X.-b. Wang, T. Tanamoto, and F. Nori, *Phys. Rev. A* **75**, 052319 (2007).
- [50] G. Vallone, E. Pomarico, F. De Martini, and P. Mataloni, *Phys. Rev. A* **78**, 042335 (2008).
- [51] H. J. Briegel and R. Raussendorf, *Phys. Rev. Lett.* **86**, 910 (2001).
- [52] H. Wang, C.-P. Yang, and F. Nori, *Phys. Rev. A* **81**, 052332 (2010).
- [53] M. Varnava, D. E. Browne, and T. Rudolph, *Phys. Rev. Lett.* **97**, 120501 (2006).
- [54] M. Hein, W. Dür, and H.-J. Briegel, *Phys. Rev. A* **71**, 032350 (2005).
- [55] F. Reiter, D. Reeb, and A. S. Sørensen, *Phys. Rev. Lett.* **117**, 040501 (2016).
- [56] X.-K. Song, Q. Ai, J. Qiu, and F.-G. Deng, *Phys. Rev. A* **93**, 052324 (2016).
- [57] J. Cho and H.-W. Lee, *Phys. Rev. Lett.* **95**, 160501 (2005).
- [58] K. Inaba, Y. Tokunaga, K. Tamaki, K. Igeta, and M. Yamashita, *Phys. Rev. Lett.* **112**, 110501 (2014).
- [59] X. Q. Shao, J. H. Wu, and X. X. Yi, *Phys. Rev. A* **95**, 062339 (2017); X.-Y. Zhu, E. Liang, and S.-L. Su, *J. Opt. Soc. Am. B* **36**, 1937 (2019); C. Yang, D. Li, and X. Shao, *Sci. China Phys. Mech.* **62**, 110312 (2019).
- [60] S.-L. Zhu, Z. D. Wang, and P. Zanardi, *Phys. Rev. Lett.* **94**, 100502 (2005).
- [61] L. DiCarlo, M. D. Reed, L. Sun, B. R. Johnson, J. M. Chow, J. M. Gambetta, L. Frunzio, S. M. Girvin, M. H. Devoret, and R. J. Schoelkopf, *Nature (London)* **467**, 574 (2010).
- [62] S.-L. Su, F.-Q. Guo, L. Tian, X.-Y. Zhu, L.-L. Yan, E.-J. Liang, and M. Feng, *Phys. Rev. A* **101**, 012347 (2020).
- [63] T. Li, A. Miranowicz, K. Xia, and F. Nori, *Phys. Rev. A* **100**, 052302 (2019).
- [64] J.-w. Pan and A. Zeilinger, *Phys. Rev. A* **57**, 2208 (1998).
- [65] S.-W. Lee, K. Park, T. C. Ralph, and H. Jeong, *Phys. Rev. Lett.* **114**, 113603 (2015).
- [66] B. P. Williams, R. J. Sadler, and T. S. Humble, *Phys. Rev. Lett.* **118**, 050501 (2017).
- [67] Y.-H. Kang, Y.-H. Chen, Z.-C. Shi, B.-H. Huang, J. Song, and Y. Xia, *Phys. Rev. A* **96**, 022304 (2017).
- [68] M. V. Berry and M. Wilkinson, *Proc. Roy. Soc. Lond. A Math. Phys. Sci.* **392**, 15 (1984).

- [69] F. Wilczek and A. Zee, *Phys. Rev. Lett.* **52**, 2111 (1984).
- [70] Y. Aharonov and J. Anandan, *Phys. Rev. Lett.* **58**, 1593 (1987).
- [71] P. Zanardi and M. Rasetti, *Phys. Lett. A* **264**, 94 (1999).
- [72] V. V. Albert, C. Shu, S. Krastanov, C. Shen, R.-B. Liu, Z.-B. Yang, R. J. Schoelkopf, M. Mirrahimi, M. H. Devoret, and L. Jiang, *Phys. Rev. Lett.* **116**, 140502 (2016).
- [73] S.-L. Zhu and Z. D. Wang, *Phys. Rev. Lett.* **89**, 097902 (2002).
- [74] W. Xiang-Bin and M. Keiji, *Phys. Rev. Lett.* **87**, 097901 (2001).
- [75] L.-M. Duan, J. I. Cirac, and P. Zoller, *Science* **292**, 1695 (2001).
- [76] E. Sjöqvist, D. M. Tong, L. M. Andersson, B. Hessmo, M. Johansson, and K. Singh, *New J. Phys.* **14**, 103035 (2012).
- [77] G. F. Xu, J. Zhang, D. M. Tong, E. Sjöqvist, and L. C. Kwek, *Phys. Rev. Lett.* **109**, 170501 (2012).
- [78] Z.-Y. Xue, J. Zhou, and Z. D. Wang, *Phys. Rev. A* **92**, 022320 (2015).
- [79] Z.-P. Hong, B.-J. Liu, J.-Q. Cai, X.-D. Zhang, Y. Hu, Z. D. Wang, and Z.-Y. Xue, *Phys. Rev. A* **97**, 022332 (2018).
- [80] Y. Xu, W. Cai, Y. Ma, X. Mu, L. Hu, T. Chen, H. Wang, Y. P. Song, Z.-Y. Xue, Z.-q. Yin, and L. Sun, *Phys. Rev. Lett.* **121**, 110501 (2018).
- [81] Z. Zhu, T. Chen, X. Yang, J. Bian, Z.-Y. Xue, and X. Peng, *Phys. Rev. Appl.* **12**, 024024 (2019).
- [82] G. F. Xu, C. L. Liu, P. Z. Zhao, and D. M. Tong, *Phys. Rev. A* **92**, 052302 (2015).
- [83] E. Sjöqvist, *Phys. Lett. A* **380**, 65 (2016).
- [84] P. Z. Zhao, G. F. Xu, Q. M. Ding, E. Sjöqvist, and D. M. Tong, *Phys. Rev. A* **95**, 062310 (2017).
- [85] J. Zhang, L.-C. Kwek, E. Sjöqvist, D. M. Tong, and P. Zanardi, *Phys. Rev. A* **89**, 042302 (2014).
- [86] B.-J. Liu, X.-K. Song, Z.-Y. Xue, X. Wang, and M.-H. Yung, *Phys. Rev. Lett.* **123**, 100501 (2019).
- [87] J. Niu, B.-J. Liu, Y. Zhou, T. Yan, W. Huang, W. Liu, L. Zhang, H. Jia, S. Liu, M.-H. Yung, Y. Chen, and D. Yu, [arXiv:1912.10927](https://arxiv.org/abs/1912.10927).
- [88] C. H. Bennett, G. Brassard, C. Crépeau, R. Jozsa, A. Peres, and W. K. Wootters, *Phys. Rev. Lett.* **70**, 1895 (1993).
- [89] C. H. Bennett and S. J. Wiesner, *Phys. Rev. Lett.* **69**, 2881 (1992).
- [90] C.-P. Shen, J.-L. Wu, S.-L. Su, and E. Liang, *Opt. Lett.* **44**, 2036 (2019).
- [91] R.-H. Zheng, Y.-H. Kang, S.-L. Su, J. Song, and Y. Xia, *Phys. Rev. A* **102**, 012609 (2020).
- [92] K. Singer, J. Stanojevic, M. Weidemüller, and R. Côté, *J. Phys. B: At. Mol. Opt. Phys.* **38**, S295 (2005).
- [93] I. I. Beterov, I. I. Ryabtsev, D. B. Tretyakov, and V. M. Entin, *Phys. Rev. A* **79**, 052504 (2009).